https://doi.org/10.5194/egusphere-2025-3527
Preprint. Discussion started: 30 July 2025

Characteristics of ocean mesoscale eddies in the Canadian Basin from a high resolution pan-Arctic model

Noémie Planat[1], Carolina O. Dufour[1,2], Camille Lique[2], Jan K. Rieck[1], Claude Talandier[2], and L. Bruno Tremblay[1]

[1]McGill University, Departement of Atmospheric and Oceanic Sciences, Montréal, Québec, Canada
[2]University of Brest, CNRS, Ifremer, IRD, Laboratoire d'Océanographie Physique et Spatiale (LOPS), IUEM, F29280, Plouzané, France

Correspondence: Noémie Planat (noemie.planat@mail.mcgill.ca)

Abstract. Mesoscale eddies are ubiquitous in the Arctic Ocean and are expected to become more numerous and energetic as sea ice continues to decline. Yet, the spatio-temporal characteristics of these eddies are poorly documented. Here, we apply an eddy detection and tracking method to investigate mesoscale eddies in the Canadian Basin over the period 1995-2020 from the output of a high resolution (1/12°) regional model of the Arctic - North Atlantic. Over that period, about 6,250 eddies are detected per year and per depth level and are distributed about equally between cyclones and anticyclones. On average, these eddies last 10 days, travel 11 km and have a radius of 12.1 km. These statistics hide strong regional and temporal disparities within the eddy population studied. In the top 85 m, the seasonal, decadal and interannual variability in the number of eddies and in their mean characteristics follow that of the sea ice cover. In contrast, below the upper pycnocline, the eddy number and properties show a weakened seasonality. At all depths, eddy characteristics and generation rate show a strong asymmetry between the slope and the centre of the Canadian Basin. The upper 85 m show an increase in the number of eddies generated along the slope, while a net diminution of the number of eddies generated is visible within the pycnocline layer along the slope presumably due to the stabilizing effect of the slope. An increased number of eddies are generated in the vicinity of the cyclonic boundary current in the AW layer. The vast majority of eddies have no temperature signature with respect to their environment, although a significant portion of long-lived eddies, located along the Chukchi shelf break, have a non-negligible temperature anomaly and penetrate into the Beaufort Gyre, thus suggesting a mechanism for the penetration of heat into the gyre. The number of eddies generated within the upper 85 m increases by 34% over the 25 year of simulation, with the largest increase occurring in the open ocean and marginal ice zone. The number of eddies between the upper and lower pycnoclines increases by 45%, with a strong year-long increase in 2008, presumably in response to the Beaufort Gyre spin-up in 2007-2008. The number of eddies in the Atlantic Waters (AW) layer shows an overall increase of 41% with little interannual variability. Finally, the analysis shows that the dominance of anticyclonic eddies within the Beaufort Gyre reported from measurements with Ice Tethered Profilers is partly due to a spatial sampling bias. This model-based eddy census can thus help interpret some of the discrepancies found between observational studies by providing a consistent spatio-temporal characterization of mesoscale eddies in the Canadian basin.

https://doi.org/10.5194/egusphere-2025-3527
Preprint. Discussion started: 30 July 2025

1 Introduction

Observations and numerical models reveal that mesoscale eddies are ubiquitous in the Arctic Ocean, including under sea ice (e.g. Manley and Hunkins, 1985; Cassianides et al., 2023; Liu et al., 2024). These eddies are thought to play an important role in the transport of heat, salt and nutrients from the shelves to the deep basins (Watanabe, 2011; Watanabe et al., 2014; Spall et al., 2008; Pickart et al., 2005) and possibly in the modulation of the marginal ice zone (MIZ; Gupta et al., 2024; Martínez-Moreno et al., 2024; Manucharyan and Thompson, 2022). In the Canadian basin, mesoscale eddies are also hypothesized to be a key component of the dynamical equilibrium of the large scale circulation through the dissipation of potential energy that accumulates within the anticyclonic Beaufort Gyre (BG, Manucharyan et al., 2016; Manucharyan and Spall, 2016; Meneghello et al., 2020; Armitage et al., 2020). Future projections of the Arctic show an increasingly energetic ocean with enhanced eddy activity (Li et al., 2024; von Appen et al., 2022) as the anticyclonic mean circulation gets stronger (Muilwijk et al., 2024) and sea ice gets thinner, less concentrated, and more mobile (Meredith et al., 2001; Meier and Stroeve, 2022). It thus appears important to document the spatio-temporal characteristics of mesoscale eddies in the changing Canadian Basin to further our understanding of the physical mechanisms controlling their generation and dissipation and of their role in the dynamics and tracer transport.

Over the past two decades, Ice Tethered Profilers (ITPs; Toole et al., 2011) and moorings deployed as part of the Beaufort Gyre Exploration Project (https://www.whoi.edu/beaufortgyre) have enabled some characterization of mesoscale and submesoscale coherent eddies from either density and temperature anomalies (Zhao et al., 2014, 2016) or Potential Vorticity (PV) anomalies (Cassianides et al., 2023). The latter study reports $O(500)$ eddies from approximately 130,000 profiles across the Arctic between 2004 and 2019, among which 87% are in the Canadian Basin, with the majority lying within the halocline (50-300 m). Eddies detected from PV anomalies within the top 700 m comprise 67% vortices with a cold core and 9% with a warm core. The documented eddies are predominantly anticyclonic ($> 95\%$), a ratio also reported in Zhao et al. (2014). Radii are observed to range from 3-15 km for analyses based on ITP profiles and from 3-80 km for analyses based on mooring profiles. No seasonality in the number of eddies or in their properties is observed, and the discussion on the interannual variability is made difficult by the temporal variability of the number of ITP profiles across the last two decades.

As opposed to the localized in-situ observations, satellite imagery offers a larger scale description of the eddy field based on surface signatures of eddies. Analyses of synthetic aperture radar data from 2007, 2011 and 2016 in the Western Arctic identify more than 7,500 eddies with diameters ranging from 0.5 km to 100 km, with cyclones twice as numerous as anticyclones, a result that strongly contrasts with the predominance of anticyclones observed from in-situ observations (Kozlov et al., 2019). In the same area, altimetry-based eddy detection reports 2,000 eddies ranging from 20 to 60 km in radius between 1993 and 2018, with orbital velocities ranging from $0.05 - 0.4$ m s^{-1}, and equally distributed between cyclones and anticyclones (Kubryakov et al., 2021). Finally, analyses of rotating ice floes within the MIZ of the Beaufort Gyre over the last two decades reveal order of thousands of eddy-like signatures having characteristic sizes ranging from 10 to 60 km with twice as many anticyclonic as cyclonic floes (Manucharyan et al., 2022).

https://doi.org/10.5194/egusphere-2025-3527
Preprint. Discussion started: 30 July 2025

Contrasting characteristics between in-situ-based and satellite-based eddy datasets may arise from differences in the fields sampled including in particular the depth at which eddies are detected, with ITPs and moorings sampling from the near-surface to 500-800 m while satellite-based observations can only report on features with a surface signature. Additionally, satellite observations of the eddy field are limited to the open ocean and MIZ, that mostly correspond to the shelf and shelf break areas. By design, ITPs can only sample the eddy field underneath the (pack) ice. These different observation approaches also lead to temporal biases, as, for instance, the MIZ is only found in summer in the BG. Contrasting eddy characteristics may also arise from the various detection methods used, which inherently sample different information, e.g. ITPs flowing "across" eddies *vs* moorings observing eddies passing by (Cassianides et al., 2023). Additionally, differences may also originate from biases due to the spatial resolution of instruments; e.g. altimetry-based detection are known to sample the larger part of the mesoscale eddy spectrum only (Kubryakov et al., 2021). Finally, some methods may be more sensitive to the detection of certain features. For instance, CTD cast-based and satellite-based detections of eddies more reliably detect anticyclones than cyclones, due to the stronger coherency of the former (Stegner et al., 2021; Giulivi and Gordon, 2006). Overall, considering the sparsity of observations and their inherent biases, it remains challenging to have a fully coherent description of the eddy field from observations.

Numerical models offer an alternative framework to investigate eddies and their characteristics by providing a consistent and complete dataset, although they come with limitations and biases of their own. Idealized configurations of the BG and/or of the Alaskan boundary current exhibit vortex-like mesoscale features, on average weaker and larger than the ones detected from in-situ observations or satellites ($O(100)$ km, Manucharyan and Spall, 2016; Meneghello et al., 2018; Spall et al., 2008). It remains unclear, however, how to compare these idealized-model-based results of the mesoscale eddy field with observations, in particular because these models have a limited representation of the processes that could generate mesoscale eddies (e.g. they typically lack a mixed layer). Recently, the resolution reached by realistic models has become fine enough in the Arctic to resolve at least part of the mesoscale spectrum (Regan et al., 2020; Hu et al., 2019; Wang et al., 2020). An analysis of the Eddy Kinetic Energy (EKE) in the entire Arctic Ocean in a 1 km resolution model shows peaks of EKE at 400 m depth at spatial scales of around 60 km, with 50% of the EKE being contained at scales smaller than 30 km (Liu et al., 2024), which corresponds to the upper boundary of the mesoscale range. In a $3-4$ km resolution regional model, focusing on the Canadian basin, a peak of EKE is found in 2007-2008 in response to the 2007 anomalous wind forcing leading to the spin up of the BG (Regan et al., 2020). However, these descriptions of the mesoscale eddy field through the EKE offer a statistical integrated quantity only, and does not relate directly to individual features that are comparable to that detected from satellite or in situ observations. Additionally, by documenting the mesoscale transient eddy field through the analysis of the EKE, these studies take into account variability at all spatial scales, including large scale (but transient) features such as e.g. meanders of the mean currents.

In this paper, we propose a census of mesoscale vortex-like features (eddies) that develop in the Canadian Basin along with a documentation of their spatio-temporal characteristics. The Canadian basin is defined as the region between 69-85°N and $108-180$°W, thus fully encompassing the BG and its surrounding area. Note that we also define the Canada Basin,

https://doi.org/10.5194/egusphere-2025-3527
Preprint. Discussion started: 30 July 2025

abbreviated CB, between $73-77°$N and $135-152°$W, as a specific region of the BG for analysis purposes (see Fig. 1). We perform a detection and tracking of eddies simulated by a 3-4 km regional model of the Arctic Ocean over the period 1995-2020. This census aims to facilitate the comparison with observations and the documentation of the eddy properties, and the implementation of the Lagrangian framework allows to discuss the displacement of eddies within the basin. The paper is organized as follows. The model and the eddy detection and tracking algorithm are described in Section 2. The spatio-temporal eddy census is presented in Section 3. A discussion of key differences with observations is offered in Section 4 together with the main findings of this study and future perspectives.

2 Methods

2.1 The pan-Arctic high-resolution model CREG12

2.1.1 Model and simulation

We use an updated version of the $1/12°$ regional Arctic-North Atlantic configuration CREG12 (Canadian Regional; Dupont et al., 2015). CREG12 runs with the ocean modelling platform Nucleus for European Modelling of the Ocean (NEMO) version 4.2.2 (Madec et al., 2023). The model is run on an ORCA12 seamless regional grid with horizontal resolution $\approx 3-4$ km in the central Arctic (Barnier et al., 2014). It uses a z* vertical coordinate with 75 levels spaced by 1 m at the surface and 150 m at 1500 m. This relatively fine horizontal grid size allows for an explicit resolution of mesoscale eddies within the deep basins where the first Rossby radius of deformation R_o is $\approx 10-15$ km, but not over the continental slope and shelf where $R_o < 7$ km (Nurser and Bacon, 2013). This configuration includes a third order momentum flux formulation, a second order scheme for tracers advection, with an additional bi-Laplacian viscosity, diffusivity formulation depending on the local velocity and a turbulence closure scheme for vertical mixing. The representation of tidal mixing effects is included in the comprehensive parameterization of mixing by breaking internal tides and lee waves (De Lavergne et al., 2016). The ocean component is coupled to the Sea Ice modelling Integrated Initiative 3 (SI3) sea ice model, with levitating sea ice that uses five categories of ice and two layers of snow (Vancoppenolle et al., 2023). The simulation is initialized in 1979 from the World Ocean Atlas 2009 for temperature (Levitus et al., 2010) and salinity (Antonov et al., 2010) with the ocean at rest and is run until 2020. Sea ice conditions are initialized from the Pan-Arctic Ice Ocean Modeling and Assimilation System (PIOMAS) (Zhang and Rothrock, 2003). The ocean and sea ice are forced with hourly atmospheric fields from the European Centre for Medium-Range Weather Forecasts Reanalysis version 5 (ERA5, Hersbach et al., 2020). The open boundary conditions at Bering Strait and along 27°N in the Atlantic are specified daily from the output of GLORYS12V1, a global reanalysis at $1/12°$ resolution run from 1993 to 2020 (Lellouche et al., 2018). Prior to 1993, output of GLORYS12V1 between 1993 and 2021 are used to build a climatology and force the open boundaries of CREG12. At Bering Strait, meridional velocities are adjusted to constrain the inflow to about 1.4 Sv, a value close to observations (Woodgate, 2018). The river run-off and Greenland melting are specified from the HYDRO re-analysis (Stadnyk et al., 2021). For additional details on the run, the reader is referred to Talandier and Lique (2024).

https://doi.org/10.5194/egusphere-2025-3527
Preprint. Discussion started: 30 July 2025

2.1.2 Evaluation of the simulation

We present here a brief evaluation of the model's representation of the hydrography, circulation and sea ice conditions in the Canadian Basin. For a more in-depth assessment of the model's performance, the reader is referred to Regan et al. (2020) and Barton et al. (2022) who use similar configurations. In this study, we focus on the period 1995-2020 to let the model equilibrate between 1979 and 1994. Over the period of analysis, the mean September sea ice cover is comparable to that derived from satellite observations (Fig. 1a,b) with small differences in summer on the Eurasian shelf and a low bias in the western CB. The modelled geostrophic circulation at the surface, related to the gradients of Sea Surface Height (SSH), shows comparable pattern and intensity than observations for the BG (anticyclonic) and for the circulation in the Nansen Basin (cyclonic, Fig. 1c,d).Within the CB, CREG12 successfully presents the vertical distribution of temperature extrema associated with the three main water masses present in this region (Fig. 1e,f), namely the summer Pacific Waters (sPW; temperature maximum at 100 m), the winter Pacific Water (wPW; temperature minimum at 200 m), and the Atlantic Water (AW; temperature maximum at 550 m). Small biases in the magnitude of the temperature extrema themselves (warm bias for the wPW, and cold bias for the sPW and AW) are noted. Despite a high salinity bias at the surface in CREG12, the modelled stratification, that allows and sustains this vertical temperature structure, displays the so-called "bowl shape" of the BG visible through the tilted isopycnals along the edges of the gyre, although slightly weaker in the northernmost side of the BG in CREG12. The model offers overall a reasonable representation of the main circulation features, with the anticyclonic BG extending down to ≈ 250 m and intensifying along the Chukchi shelf break (see the Mean Kinetic Energy (MKE) in Fig. A1). The cyclonic boundary current within the AW layer is found around the CB at 500 m with a returning branch of weaker intensity along the Canadian Archipelago (Fig. A1c). Upper outflows through the Canadian Archipelago are similar to observation-based derived circulation (see Fig. A1, see also Planat et al., 2024). Analyses of EKE shows an intensification along the shelf break and along topographic features such as Northwind Ridge (NWR), with a more quiescent deep basin by one to two orders of magnitude, in line with mooring-based estimates of EKE (Fig. 2a,b, see also von Appen et al., 2022).

2.2 Detection and tracking of mesoscale eddies

2.2.1 Detection

We perform an offline detection and tracking of mesoscale eddies within the Canadian Basin over 1995-2020. Our definition of *eddies* spans here a broad range of mesoscale rotating features, from the evanescent vortices quickly dissipated by sea ice to the more persistent features that may eventually evolve into materially coherent vortices. This broad definition thus includes parts of the "turbulent soup" that is expected to develop at the surface in response to the atmospheric and ice forcings and should be captured by the model. Though short-lived, these features which are characteristic of the surface ocean, deserve an investigation as they allow to investigate the energy dissipation exerted by sea ice and participate to the energetic equilibrium of the basin. In the following, we focus on features with characteristic sizes from $R_0 \approx 10$ km to $2\pi R_0 \approx 60$ km (defining the mesoscale, e.g. Tulloch et al., 2011).

To identify eddies, we use the *eddytools* python package documented in Rieck et al. (2024). Eddies are detected using the

https://doi.org/10.5194/egusphere-2025-3527
Preprint. Discussion started: 30 July 2025

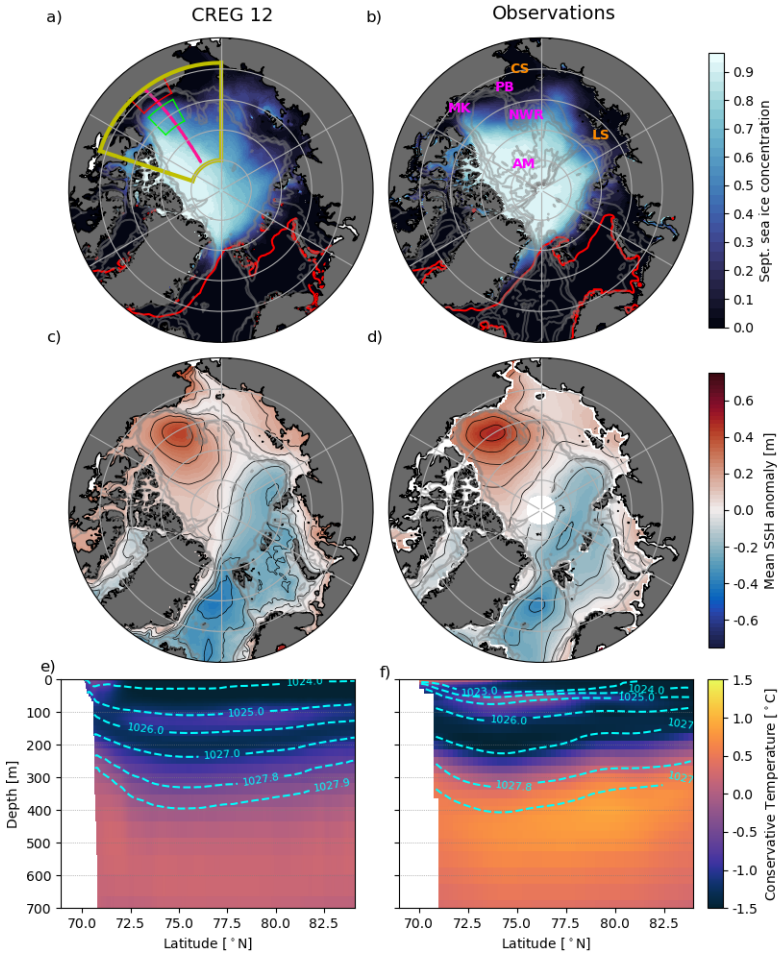

Figure 1. Mean sea ice concentration in September (background color) and in March (80 % contour in red) over 1995-2020 from (a) CREG12 and (b) National Snow and Ice Data Center (NSIDC) Climate Data Record (DiGirolamo et al., 2022), a blend between the NASA-Team algorithms (Cavalieri et al., 1984) and the NASA Bootstrap algorithm (Comiso, 1986). Mean Sea Surface Height (SSH) anomaly with respect to the mean over 2011-2020 and above 65°N from (c) CREG12 and (d) the updated altimetry-based product of Armitage et al. (2016). Black contours are evenly spaced every 0.1 m between −0.75 m and 0.75 m. Mean conservative temperature (background) and potential density referenced to surface (dashed contours) along a transect at −145°E over 2005-2014 from (e) CREG12 and (f) World Ocean Atlas 2023 climatology. Note the different periods displayed for each variable to match that of the observation datasets. Boxes on panel a) represent the regions used for our analyses corresponding to the Alaskan shelf area (red) and the Canada Basin (CB, green). The thick yellow box indicates the Canadian Basin i.e. the entire domain analysed in this study. The pink line is the section used for Fig. D1. In panel b), CS and LS stand from Chukchi and Laptev Sea, respectively, and NWR, PB, AM and MK for Northwind Ridge, Pt. Barrow, Alpha-Mendeleev Ridge and McKenzie River respectively. Thin gray lines show the bathymetry, respectively 100, 500 and 1000 m depth isobaths on (a), (c), (d) and 100, 500 , 1000, 2000 and 3000 m depth isobaths on (b).

https://doi.org/10.5194/egusphere-2025-3527
Preprint. Discussion started: 30 July 2025

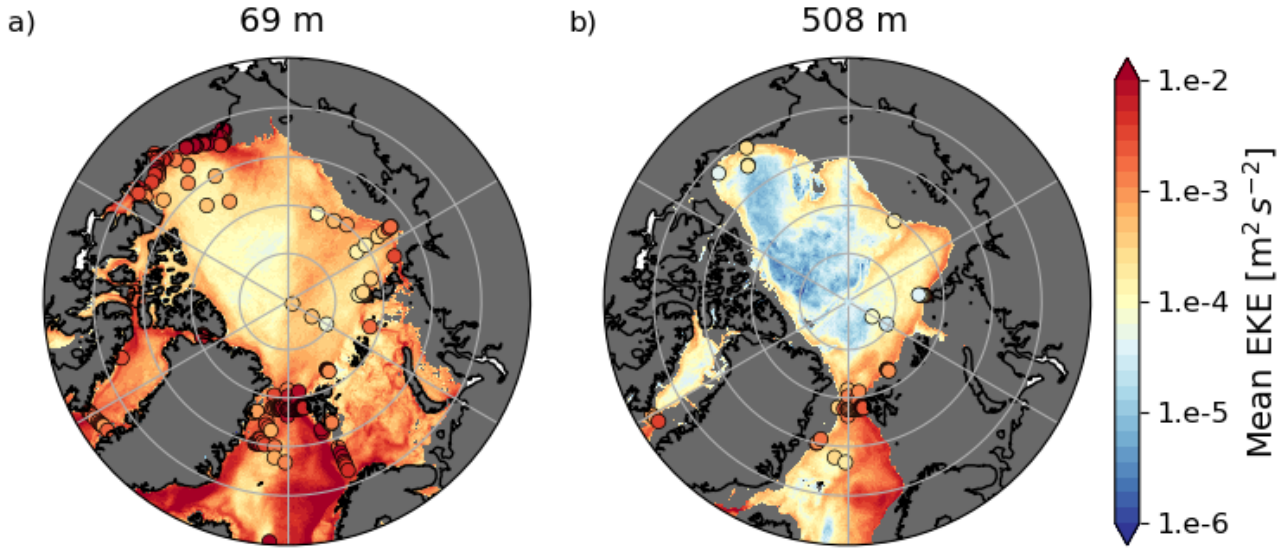

Figure 2. Eddy Kinetic Energy (EKE) computed from velocity anomalies with respect to the monthly means in CREG12 and averaged over the 26 years of simulation (a) at 69 m (within the halocline) and (b) at 508 m (within the AW layer). Super-imposed are mooring-based estimates of EKE from von Appen et al. (2022), computed similarly from monthly mean anomalies. The reader is referred to von Appen et al. (2022) for exact calculation method.

Okubo-Weiss parameter (OW; Okubo, 1970; Weiss, 1991), which measures the relative importance of shear and strain to vorticity (Fig. 3a) in the velocity field:

$$\mathrm{OW} = (\partial_\mathrm{x}\mathrm{u} - \partial_\mathrm{y}\mathrm{v})^2 + (\partial_\mathrm{x}\mathrm{v} + \partial_\mathrm{y}\mathrm{u})^2 - (\partial_\mathrm{x}\mathrm{v} - \partial_\mathrm{y}\mathrm{u})^2 \quad (1)$$

where u, v denote the velocities along the x and y directions of the grid, locally orthogonal. The resulting OW field (Fig. 3b) is compared to the local OW standard deviation ($\sigma_{\mathrm{OW}}(x, y)$) averaged over the full time period (Fig. 3c). σ_{OW} is computed over a $L_\sigma \times L_\sigma$ box, L_σ being chosen small enough to capture the regional differences between e.g. the centre of the gyre and the boundary currents, but large enough so that σ_{OW} is not impacted by individual eddies. To be retained, eddies have to meet the following condition :

$$\mathrm{OW}(\mathrm{x},\mathrm{y},\mathrm{t}) < -\alpha\sigma_{\mathrm{OW}}(\mathrm{x},\mathrm{y}) \quad (2)$$

where α is a threshold value typically chosen between 0.2 and 0.5 (Isern-Fontanet et al., 2003; Chelton et al., 2007; Pasquero et al., 2001; Rieck et al., 2024). The detection is implemented using daily-averaged output in the Canadian Basin. The detection is run for each vertical level of the model independently above 1200 m (which represents a lower bound of the AW layer) totalling 49 levels. Connecting the results between the vertical layers is not trivial and no 3D representation of eddies is attempted here. Note that because σ_{OW} is computed independently for each depth level, the minimum OW used to identify an

https://doi.org/10.5194/egusphere-2025-3527
Preprint. Discussion started: 30 July 2025

eddy also varies with depth. In other words, at depths of intense mesoscale activity, the OW an individual eddy needs to have to be identified as such will be more extreme. For each eddy, we estimate its radius with $R = \sqrt{area/\pi}$ even though the eddies might have an elliptic shape.

We set the smallest eddies that the algorithm detects to occupy 20 grid points, which correspond to equivalent circular eddies with a minimum of 5 grid points across the diameter. A 5-grid point diameter circular structure corresponds to an eddy of 7.5 to 10 km radius, depending locally on the grid size of the model, which is the lower bound of R_0 over the deep part of the Canadian Basin (see Nurser and Bacon, 2013). On the shelf, R_0 is smaller ($\approx 2-5$ km) thus we only detect the largest mesoscale rotating features. Statistics presented here include all detected features, but remain valid when filtering out eddies on the shelf, as the vast majority of eddies are detected over the continental slope and within the basins (not shown).

Sensitivity tests for α show that the vertical distribution of the mean eddy radius, duration, polarity ($r_{C/T}$, ratio of cyclones to total number of eddies) and vorticity Ω are robust to changes of α from 0.5 to 0.1 despite changes in the total number of detected features with slightly larger, weaker and shorter eddies for smaller α (Fig. B1). For our analyses, we chose $\alpha = 0.3$ as an intermediate, and commonly used, value. The box length L_σ over which to compute σ_{OW} needs to be tuned to the main spatial scales of energy regimes in the basin. In other words, L_σ should be small enough to capture the jet-like circulation along the Alaskan and Chukchi slopes that are about $200-300$ km large and large enough to allow statistically relevant values of σ_{OW}. We argue that $L_\sigma = 200$ km is a reasonable value to resolve the different dynamical regimes within the Canadian Basin. Similarly to α, sensitivity tests indicate that changing L_σ within the range $[50, 400]$ km does not modify the vertical distribution of the mean eddy radius, duration, vorticity and polarity although the total number of detected features vary (not shown). Overall, modifications of α and L_σ impact the precise definition of particular eddies but not the statistical properties of the eddy field.

2.2.2 Tracking

Eddies are tracked over consecutive days using three main criteria: (i) their speed of propagation, (ii) their polarity, and (iii) their radius R (Fig. 3c). For each eddy detected on day *t*, if an eddy with similar radius (within $[0.5R, 1.5R]$) and same polarity lies within a search radius R_s on day *t+1*, it is chosen as a continuation of the track. In case there is more than one eddy matching these criteria, the one located the closest to the original eddy is chosen. Results do not appear sensitive to a search radius $R_s \in [15, 53]$ km, and we choose a search radius $R_s = 22$ km corresponding to a propagation speed of 25 cm/s, which is approximately the speed of the fastest simulated current within the domain, located along the Chukchi slope in summer.

The radius, location and grid-point occupied by each individual eddy are stored every day. We consider eddies to be born (generated) the first time they are detected and to be dead (dissipated) the last time they are detected. However, the algorithm may occasionally lose track of eddies, leading to a given eddy being counted as two successive eddies of similar properties. This interruption in the tracking generally occurs with weak features that are not well developed and thus not detected as eddies over consecutive days. We remove these eddies by filtering out any eddy that does not persist over at least two consecutive days. While this filtering does not fully overcome the interruption in the eddy detection – in particular if one eddy splits into two different ones, or equivalently if two eddies merge – it removes most of the issue and enables us to focus more on well-

https://doi.org/10.5194/egusphere-2025-3527
Preprint. Discussion started: 30 July 2025

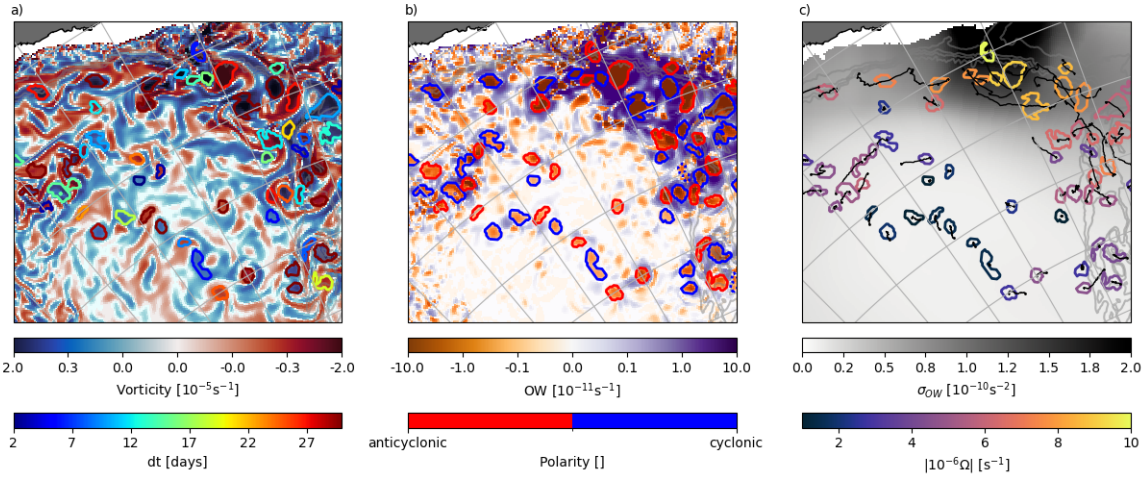

Figure 3. (a) Vorticity, (b) OW, and (c) OW standard deviation σ_{OW} for one day in September chosen randomly (here, Sept. 16th, 1996) at 30 m along the south-eastern edge of the CB. Superimposed on each panel are the detected eddies present on that day, coloured with (a) their duration, (b) their polarity (red indicating anticyclones and blue cyclones), and (c) their intensity i.e. the absolute value of the difference between the vorticity in the centre of the eddy and the average vorticity along the edge of the eddy. Plain contours on (a), (b) and (c) indicate eddies lasting more than 2 days, dotted red and blue contours on (b) indicate eddies with a duration of one day. Black thin lines on (c) indicate the eddy trajectories. Thin gray lines indicate the 100, 500, 1000 and 1500 m depth isobaths.

developed eddies. Still, the majority of eddies we detect are relatively weak and have a duration shorter than their turnaround time scale ($\tau = 2\pi/|\Omega|$). A discussion of the characteristics of the more vigorous and persistent eddies that are likely more comparable to the accepted definition of coherent mesoscale eddies is proposed in Section 4.

2.2.3 Properties

For each detected and tracked eddy, we extract or compute its absolute salinity (S), conservative temperature (T), and intensity, that we define as the absolute vorticity amplitude of the eddy i.e. the difference between the vorticity in the centre of the eddy and the average vorticity along the edge of the eddy ($|\Omega|$). We equivalently report its relative intensity $|\Omega|/f(\lambda)$ where f is the Coriolis parameter computed as a function of the latitude λ. We also extract the mean ice concentration A and thickness h above each eddy. Eddy properties are computed by spatially averaging over the eddy area and are tracked along the eddy pathway. Except where mentioned, properties are extracted at the eddy generation time. Localizations of eddies are obtained from their centre of mass - thus, the distance travelled by a given eddy between two consecutive days is possibly smaller than

https://doi.org/10.5194/egusphere-2025-3527
Preprint. Discussion started: 30 July 2025

the grid resolution if an eddy is very slow. The properties of the eddy environment are defined by spatially averaging over a box that we take to be $n = 3$ times larger than the fitted eddy width and length (thus not of identical size along both x and y directions) and from which we remove the eddy area. We note $\Delta X = X_i^{eddy} - X_i^{env}$ the anomaly of property X at the time of eddy generation i. If two eddies develop next to each other, they will become each other's environment as we do not use a 2D eddy mask. To increase the robustness of the anomaly quantification, we only report the anomalies when "significant" in the rest of the manuscript, except if mentioned. We define "significant" from the standard deviation of property X over the environment removing the eddy area, σ_X^{env} :

$$\delta X = X_i^{eddy} - X_i^{env} + \begin{cases} +\sigma_X^{env} \text{ if } \mathrm{X}_i^{eddy} - \mathrm{X}_i^{env} < 0 \\ -\sigma_X^{env} \text{ if } \mathrm{X}_i^{eddy} - \mathrm{X}_i^{env} > 0. \end{cases} \tag{3}$$

The anomaly is said significant if δX and the anomaly ΔX are of the same sign, that is if the anomaly is larger in absolute than the standard deviation over the area. Finally, the amplitude of the seasonal cycle is defined for each property X as:

$$SC_X = \frac{X_{max} - X_{min}}{\overline{X}} \tag{4}$$

where the maximum, minimum and mean are taken along the seasonal cycle.

3 Results

3.1 Characteristics of mesoscale eddies at basin scale

Over 1995-2020, we detect and track about $6,250$ eddies per model depth level and per year in the Canadian Basin. Here, we present the statistics aggregated over the whole 1995-2020 period and over all depth levels above 1,200 m, hence accounting for the same eddy several times if that eddy spans several depth levels. Most of the eddies detected in the model have a radius similar to the Rossby radius of deformation with $\bar{R} = 12.1$ km, are short lived with an averaged duration $\bar{dt} = 10$ days and do not travel far with an averaged distance travelled $\bar{D} = 11.1$ km (Fig. 4a-c). Of all eddies detected, 49% are cyclones. Cyclones and anticyclones have a similar intensity ($|\overline{\Omega}| = 4.6 \cdot 10^{-6}$ s^{-1} corresponding to a relative intensity of $\overline{|\Omega|/f} = 0.03$; Fig 4b). Temperature and salinity anomalies are found for 15% of the eddies (Fig. 4e,f). The narrow and short tail of the statistical distribution of radius ΔS indicates that the overwhelming majority of detected eddies have properties close to the mean, while the wider distribution of ΔT indicate large temperature anomalies for a significant portion of the eddy population (see box whiskers on Fig. 4 and Table 1 with numerical values of $10^{th}/90^{th}$ percentiles of each property). The eddy intensity, duration and travelled distance have a standard deviation of the same order of magnitude as the mean. The distribution of the distance travelled, in particular, shows three modes (Fig. 4b): a first one corresponding to quasi-stationary eddies, and two secondary ones centered around 4 km and 8 km. Interestingly, eddies with properties at the tail of the distributions do not represent a distinct population of eddies. For instance, larger eddies do not systematically live longer (see Fig. C1).

Statistics aggregated over the whole eddy population hide significant differences across depth. Indeed, the general shape of the distribution of eddy properties is similar at all depths, but the means and percentiles vary (see the coloured plain lines and

https://doi.org/10.5194/egusphere-2025-3527
Preprint. Discussion started: 30 July 2025

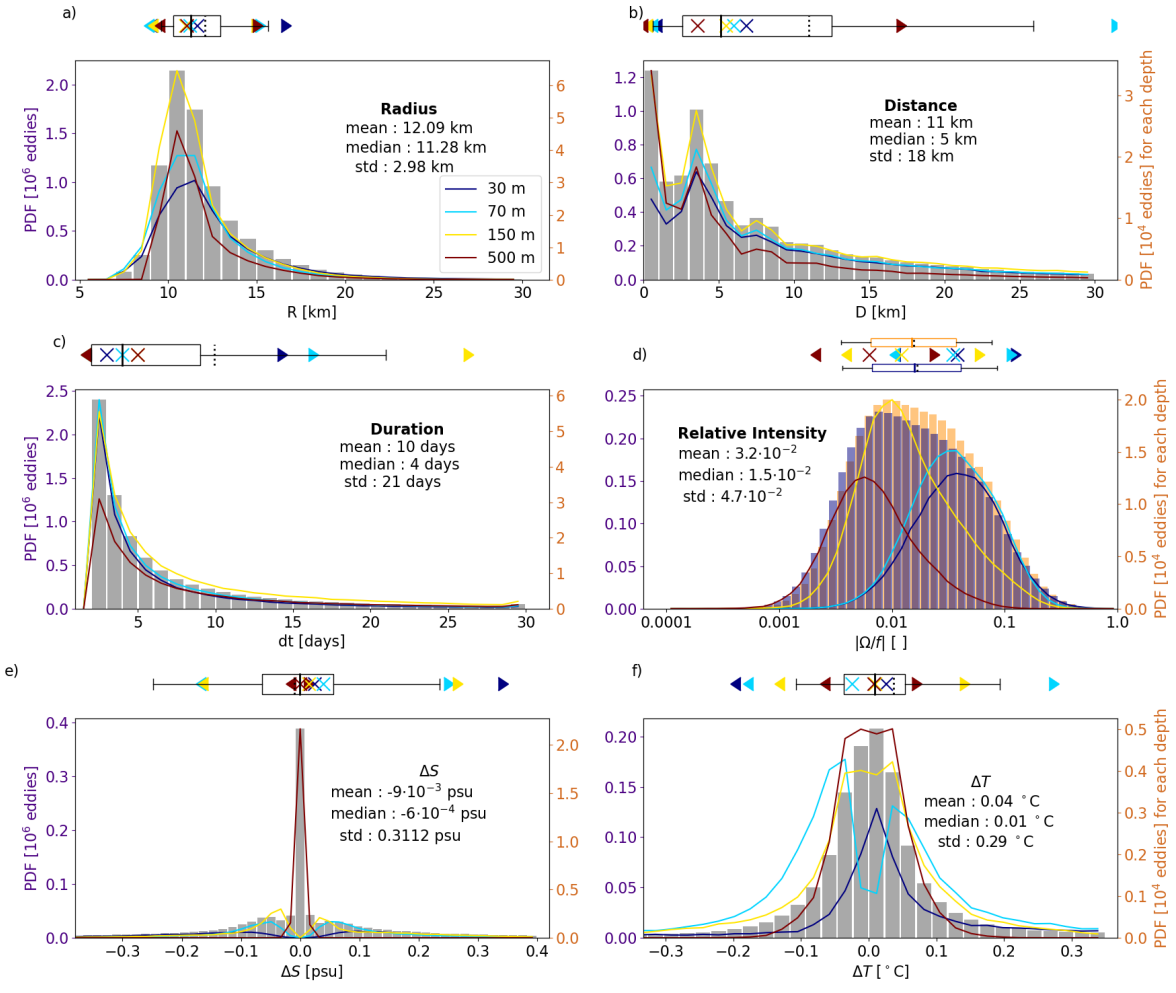

Figure 4. Histogram of the properties of eddies generated at all depths in the model: (a) radius, (b) distance travelled, (c) duration, (d) relative intensity for cyclones (blue) and anticyclones (orange), and anomalies in (e) salinity and (f) temperature with respect to the surrounding environment (see Sect. 2). All variables are estimated at the time of eddy generation that is the first time an eddy is detected. Number of eddies are reported in million along the left axis (indigo). Anomalies are only accounted for when significant (see Sect. 2), that is only $\approx 15\%$ of all eddies are considered for panels (e) and (f). Box plots indicate the quartiles Q1 and Q3, the median (plain line) and mean (dotted line), and the 10^{-th} and 90^{-th} percentiles in the whiskers. Plain lines correspond to the histogram of properties at specific depths (11 m, 30 m, 69 m, 147 m and 508 m), reported along the right axis in tens of thousands of eddies. On panel d), plain lines report the histogram of absolute relative intensity, that is, for both cyclones and anticyclones together. Coloured ◄, ► and × respectively indicate the 10^{-th}, 90^{-th} and median at the corresponding depth.

https://doi.org/10.5194/egusphere-2025-3527
Preprint. Discussion started: 30 July 2025

	Radius R	Duration dt	Distance travelled D	Intensity $\|\Omega\|$	Temperature anomaly ΔT	Salinity anomaly ΔS
10^{th} perc.	9.8 km	2 day	0.6 km	$5.7 \cdot 10^{-7}$ s^{-1}	-0.10°C	-0.25 psu
90^{th} perc.	15 km	21 days	26 km	$1.1 \cdot 10{-}5$ s^{-1}	0.20°C	0.24 psu

Table 1. Eddy characteristics defined from the 10^{th} and 90^{th} percentiles of the distribution for all eddies at all depths above 1,200 m. Percentiles of the temperature and salinity anomalies are computed on $\approx 15\%$ of the total eddy population.

◄, ► and + in Fig. 4), motivating the analysis of eddy properties with depth. To this end, we seek to define vertical layers with consistent properties. Within the top 1200 m, the total number of eddies generated at each model depth level remains roughly constant between the surface and 85 m, and below 225 m, but increases by two thirds between 85 m and 225 m (Fig. 5a). We also note important transitions in the ratio of anticyclones versus cyclones, radius and eddy durations around these depths suggesting different mechanisms of formation and dissipation. On average across the basin and along the 26 years, these transition depths correspond to the upper pycnocline (∼85 m) which is associated to the summer Pacific Waters (sPW), and to the lower pycnocline (∼225 m) which is associated to the winter Pacific Waters (wPW, see Fig. 5g,h). Based on these depths, we thus define three layers : the upper layer (0-85 m), the pycnocline layer (85-225 m) and the AW layer (225-1200 m). Next, we describe the eddy properties and discuss their formation and dissipation within each of these three layers. The results presented in the following are robust to the exact definition of the layer boundaries (± 2 depth levels).

3.2 Characteristics of eddies within the surface layer

3.2.1 Mean annual and seasonal cycle of eddy characteristics

Within the top 85 m, a total of ≈ 6000 eddies per year and per depth level are detected. The properties of these eddies show a marked seasonal cycle (Fig. 5) that mainly follows that of the sea ice cover. Note that because we only track eddies in the horizontal and not in the vertical, we cannot discriminate eddies generated within the upper layer only from eddies extending across the upper and pycnocline layers.

From winter to summer, the number of eddies increases by a factor of 10 with a minimum in April, just before the onset of sea ice melting, and a maximum in September when sea ice is at its minimum (Fig. 5a). The Mixed Layer (ML) depth – computed as the depth at which the potential density has increased by 0.01 kg m^{-3} compared to the potential density at 1 m – decreases from 35 m in January-May to 3 m in July, and increases from August to December, when it recovers 30 m (see also the stratification on Fig. 5h). The ML depth delimits different regimes of variations for the mean radius, polarity and intensity. Within the ML, the averaged radius of eddies increases from 12 km in early summer to 14 km in fall, while below the ML, the averaged radius of eddies barely changes comparatively (increase from 12 km to 12.5 km; Fig. 5b). In winter, a dominance of anticyclones is found at the surface (0-10 m) and of cyclones just below (10-40 m, i.e. to the base of the ML), while at the

https://doi.org/10.5194/egusphere-2025-3527
Preprint. Discussion started: 30 July 2025

very surface eddies are essentially anticyclonic year long (Fig. 5d). This dipole structure in winter results from a dominance of anticyclones at the very surface (upper 10 m) within the Canada basin year long and cyclones within the Chukchi shelf break area in winter (not shown). Below the base of the ML, the proportion between cyclones and anticyclones remains more equally distributed throughout the year with about 55% anticyclones. Within the top 85 m, intense eddies are found during the stratification and de-stratification periods (onsets of sea ice growth (October and November) and melt season (May-July), respectively) as well as at the based of the ML in winter (Fig. 5c).

Eddies persist longer in summer ($7-8$ days) than in winter when their duration is reduced by about half (Fig. 5e). Durations likely influence distance travelled, with eddies propagating over $15-16$ km in summer and $7-8$ km in winter on average (Fig. 5f). We find eddy durations to be similar to the characteristic times of spin-down through sea ice dissipation when sea ice is taken as the main drag (e.g. Meneghello et al., 2021; Pedlosky, 1982). Yet, vast majority of eddy durations are significantly smaller than the theoretical mean turnaround time (85%). Thus, part of the closed and somewhat circular features that we detect are likely not fully developed structures but rather belong to the "turbulent soup" that is generated in response to the surface density gradients and gets quickly dissipated by sea ice in winter. We come back to this distinction in Sect. 4.

3.2.2 Spatial distribution of eddy characteristics

Eddy properties present large variations across the Canadian Basin (Fig. 6). In particular, there is a strong contrast between the continental slope and the deep basin, with up to 10 times on average more individual eddies detected over the relatively small area that the slope represents ($\approx$ 150 km wide, Fig. 6a). The greater generation of eddies over the slope peaks in October, when sea ice extent is close to its minimum and winds start to increase (see Fig. D1). While the production of eddies in the CB remains low on average, it becomes similar to the production over the slope when sea ice concentration drops below $\approx 80\%$, that is between July and November depending on the latitude (see Fig. D1a). Simultaneously, eddy duration increases from evanescent below the pack in winter to about 15 days in summer on average (Fig. D1b). Yet, over the domain, eddy duration shows little spatial variability (not shown). Up to 300 km off the shelf, high levels of eddy production are accompanied by intensities in the eddy field up to one order of magnitude higher than in the deep basin (Fig. 6c). This is visible all along the shelf break of the domain, that is from the Alpha-Mendeleev Ridge to Chukchi shelf break. Over the slope, eddies have, on average, a positive temperature anomaly ($\approx 0.3°$C) with the exception of some anomalously cold eddies forming over the Chukchi shelf. Where the mean September sea ice concentration is higher than 15%, eddies have no temperature anomaly. We also find a contrast in radius between the eastern and western side of the gyre, especially off-shore the Chukchi shelf break and above NWR, where eddies are found to be about 60% larger (Fig. 6b). These eddies have an intermediate intensity and generation rate, and are located within intense anticyclonic BG circulation (Fig. A1) and therefore travel up to 40 km throughout their duration (to be contrasted with the averaged distance travelled of 8 km within the CB).

Anticyclones are predominant over the centre of the gyre, while over the slope, a greater proportion of cyclones are found. (Fig. 6d). The investigation of vorticity anomalies within the CB does not indicate any preference for the generation of anticyclones (not shown). One hypothesis to explain this cyclone/anticyclone asymmetry, suggested in the Mediterranean Sea and more generally in other contexts of turbulent flows, is that anticyclones are more persistent than cyclones that tend to split in

https://doi.org/10.5194/egusphere-2025-3527
Preprint. Discussion started: 30 July 2025

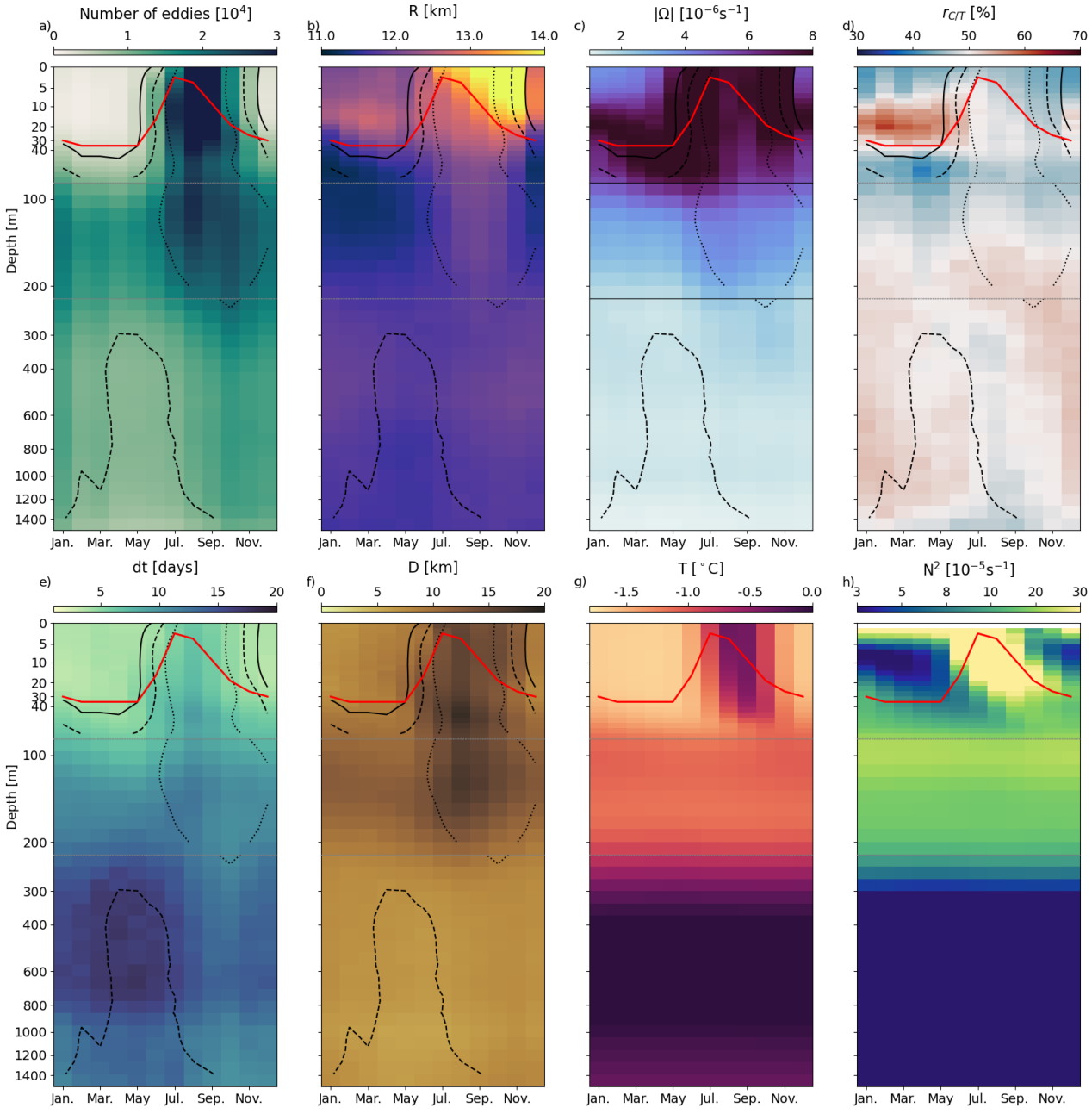

Figure 5. Seasonal cycle of eddy and basin properties with depth. (a) The number of eddies generated within each model depth level and month summed over the 26 year of simulation, and associated averaged properties: (b) radius, (c) intensity, (d) polarity $r_{C/T}$ i.e. the ratio of the number of cyclones to the total number of eddies, (e) duration, (f) distance travelled. Basin-averaged (g) potential temperature and (h) stratification (N^2). For panels b-h, properties are averaged at each model depth level and month over the 26 years of simulation. For panels a-f, dotted, dashed and plain lines indicate the iso-contours corresponding to $5,000$ $10,000$ and $20,000$ eddies as calculated in (a), thus indicating where the statistics might be less robust due to the lower number of eddies. Note the use of a non-linear vertical axis to highlight the variability in the upper layer. Dotted horizontal grey lines delineate the three regions introduced in Section 3: upper layer, pycnocline layer and Atlantic Waters layer. The red line indicates the depth of the base of the mixed layer (ML) computed from a potential density threshold referenced to 1 m of 0.01 kg m^{-3}.

https://doi.org/10.5194/egusphere-2025-3527
Preprint. Discussion started: 30 July 2025

smaller objects, leading to anticyclones being more systematically identified in the datasets (Stegner et al., 2021; Giulivi and Gordon, 2006). Beech et al. (2025) further suggest the role of sea ice in filtering small cyclones. Whether this applies to the BG is worth future investigation. In particular, we suggest such mechanism is mainly visible in the centre of the gyre where the turbulent field is dominant while near the edges, strong mean currents can lead to faster dissipation/destruction of eddies regardless of their polarity.

The most intense eddies are found at the mouth of the McKenzie River and at Pt. Barrow (not shown), being respectively fresher and saltier than their environment (Fig. 6e,f). Along the Alaskan and Chukchi slopes, on both sides of Pt. Barrow, eddies with positive salinity anomalies are detected in the inner part of the slope while eddies with negative anomalies are detected in the outer part. This pattern illustrates the penetration of the Pacific Waters from Pt. Barrow along the baroclinically unstable Alaskan coastal and Chukchi Slope currents (Corlett and Pickart, 2017; Spall et al., 2008) and supports the observations of the penetration of anomalously salty eddies into the Canada Basin made at Pt. Barrow (MacKinnon et al., 2021, in the submesoscale range). The elongated band of negative anomalies on the other hand confirm the role of fresh water input from McKenzie River in generating instabilities along the anticyclonic circulation producing anomalously fresh eddies downstream (Kubryakov et al., 2021).

3.2.3 Decadal and interannual variability of eddy generation

Over 1995-2020, the September sea ice extent decreases by 55% in the Canadian Basin while the number of eddies generated in that region increases by 34% (comparison between the first and last 5 years of the layer-averaged number of eddies relative to the 26-years average ; Fig. 7). Similar increases in the eddy number are found when looking regionally at the CB ($+31\%$) and the Alaskan shelf area ($+47\%$). A key difference between the two areas is that the CB is mostly energized above the mixed layer ($+94\%$ above 30 m *vs* -15% between 30 and 85 m). In contrast, the Alaskan shelf presents an increase in the number of eddies that is roughly constant with depth throughout the upper layer.

As sea ice shrinks, the number of eddies is expected to increase over the domain, as suggested by studies reporting on an enhancement of the EKE over the Arctic. Yet, it is unclear whether the increase in the EKE is due only to the expansion of the open ocean and the MIZ, thus allowing for a higher transfer of energy from the atmosphere to the ocean, or a reduced dissipation from the sea ice (Muilwijk et al., 2024; Li et al., 2024; Rieck et al., 2025). To investigate this question, we look at the eddy density within three sea ice regions in the upper layer our domain : the pack ice (where the ice concentration is $\geq 80\%$), the MIZ and the open ocean (where the ice concentration is $\leq 15\%$). For a given year and sea ice region, the eddy density is defined as the total number of individual eddies detected (for that year) over the sea ice area cumulated for that year in that region. Over the 26 years, we find an increase of $+10\%$ and $+20\%$ of the eddy density in the open ocean and MIZ respectively, and a slight decrease of -2% below the pack ice (Fig. G1). The small decrease of eddy density in the pack ice results from an increase above the ML of $+10\%$ and a decrease of similar amplitude below. This increase in eddy generation in the MIZ and Open Ocean points to an enhancement of eddy generation presumably through the additional energy penetrating into the ocean in line with the results of Li et al. (2024). Our results thus suggest that the number of eddies do not only increase because of an expansion of the open ocean area but also because of the energy injection in all regions of the domain, although

https://doi.org/10.5194/egusphere-2025-3527
Preprint. Discussion started: 30 July 2025

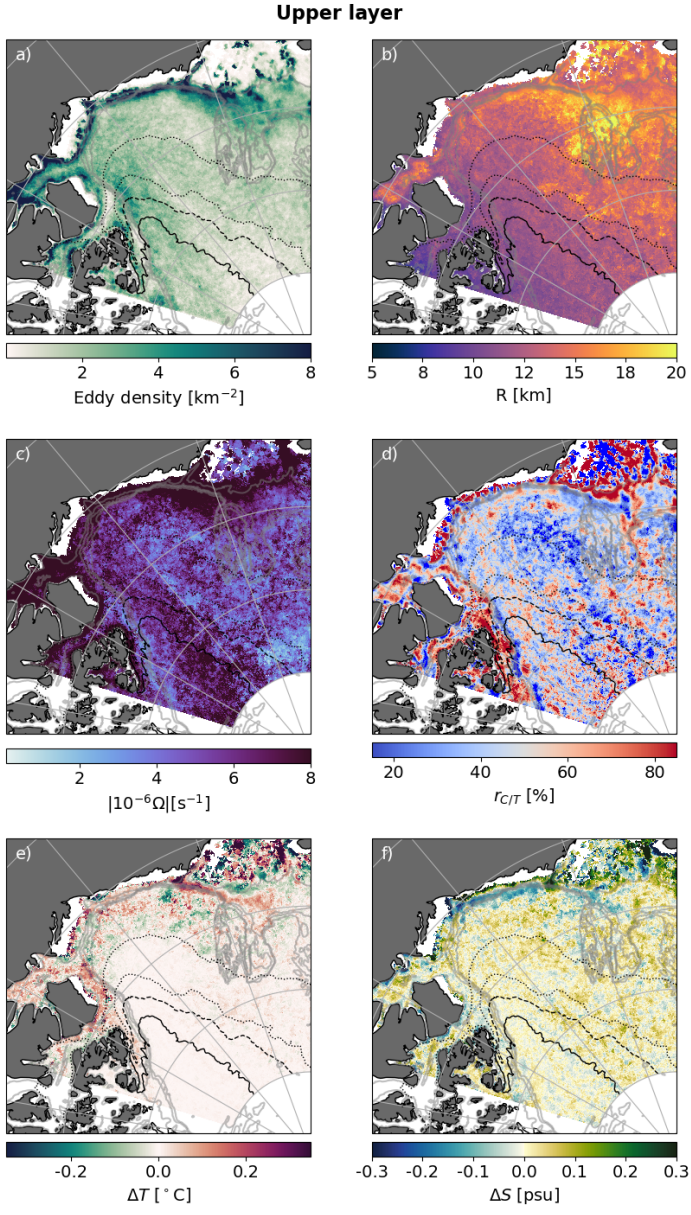

Figure 6. Eddy properties in the upper layer (at 30 m) over the 26 years of simulation. (a) Eddy density (i.e. number of individual eddies detected per km^2) and associated properties: (b) averaged radius, (c) intensity, (d) polarity, and anomalies of (e) temperature and (f) salinity with respect to the environment of eddies where temperatures are taken with respect to the local freezing temperature. Temperature and salinity anomalies are only accounted for when respective anomalies are significant (about 15% of all eddies). All variables are extracted at nominal depth 30 m, and averaged/summed over the 26 years of simulation. Note that all fields show similar structures at all depths between 0 and 70 m except for the radii that are significantly larger within the ML (see Fig. 5c). Plain, dashed, dotted and loosely dotted black lines show respectively the 90%, 80%, 50% and 15% contours of the climatological September sea ice concentration. Gray shaded plain lines show the 100, 500, 1000, 1500 m isobaths.

https://doi.org/10.5194/egusphere-2025-3527
Preprint. Discussion started: 30 July 2025

limited to the very surface the pack ice area.

On interannual time scales, all the CB, Alaskan shelf areas and whole Canadian Basin show important variability in the number of eddies detected. Significant negative correlations ($p < 0.05$) between the detrended number of eddies generated within the upper layer and the yearly cumulated sea ice area are found over the whole domain ($r = -0.65$) and more regionally over the Alaskan shelf area ($r = -0.46$). Similar analyses across each depth level of the Canada basin show significant correlations at the very surface but these quickly become non-significant with depth. These results thus point to a local transfer of energy from the atmosphere to the ocean when the ice cover is diffuse enough, while it may take a greater time to penetrate at depth in regions that have a concentrated ice cover year-round like the CB.

3.3 Characteristics of eddies in the pycnocline layer

3.3.1 Mean annual and seasonal cycle of eddy characteristics

Over the 26 years of simulation, there are about half more eddies detected between the two pycnoclines (∼85-250 m) than in the upper layer (8,900 vs 6,000 eddies per year per depth level; Fig. 5a). Eddies detected between the two pycnoclines are evenly distributed between cyclones and anticyclones (Fig. 5d) and are found to be smaller and weaker than in the upper layer on average (mean radius is decreased from 12.4 km to 11.6 km and intensity is decreased from $7.4 \cdot 10^{-6}$ s^{-1} in the upper layer to $3.3 \cdot 10^{-6}$ s^{-1}, Fig. 5b,c). Although weaker, eddies in the pycnocline layer last about 6 days longer than in the upper layer, likely due to the absence of ice or air drag to dissipate eddies through friction (Fig. 5e). Despite this increased longevity, the mean distance travelled by eddies in the pycnocline layer is only increased by about 1.1 km compared to the upper layer (Fig. 5f), presumably because of the weaker background mean flow advecting these eddies. Therefore, of the eddies generated over the slope, only the strongest and longest-lived eddies may be able to travel far enough to reach the gyre and could thus participate in the transport of heat, salt and nutrients from the continental shelf to the deep basins (see Sect. 4).

Eddy characteristics in the pycnocline layer show a weaker seasonality compared to the upper layer. This damped seasonality is expected as the upper pycnocline at ∼70 m shields the pycnocline layer from dissipation by the sea ice. Quantitatively, the amplitude of the seasonal cycle of the number of detected eddies diminishes with depth, from $SC_N = 2.3$ at 30 m to $SC_N = 0.8$ at 85 m and $SC_N = 0.5$ at 150 m (see Sect. 2 for a definition of SC_X). The other properties also show a decreased amplitude of their seasonal cycle compared to the upper layer, by $\approx 60\%$ for the radius, 50% for the intensity and distance travelled, and by 40% for the duration (refer to Table 2 for detailed seasonal cycles).

3.3.2 Spatial distribution of eddy characteristics

For most eddy characteristics (radius, intensity, duration, distance and polarity), the spatial distribution between the two pycnoclines is generally similar to that of the upper layer (compare Fig. 6 with Fig. 8) and persist year long (including the relatively high intensity along the slope). This similarity with the upper layer is expected as the anticyclonic circulation that dominates most of the region investigated extends down to the second pycnocline (see Fig. A1, see also Planat et al., 2024). However, the spatial distribution of the eddy density in the pycnocline layer shows a different structure than in the upper layer along

https://doi.org/10.5194/egusphere-2025-3527
Preprint. Discussion started: 30 July 2025

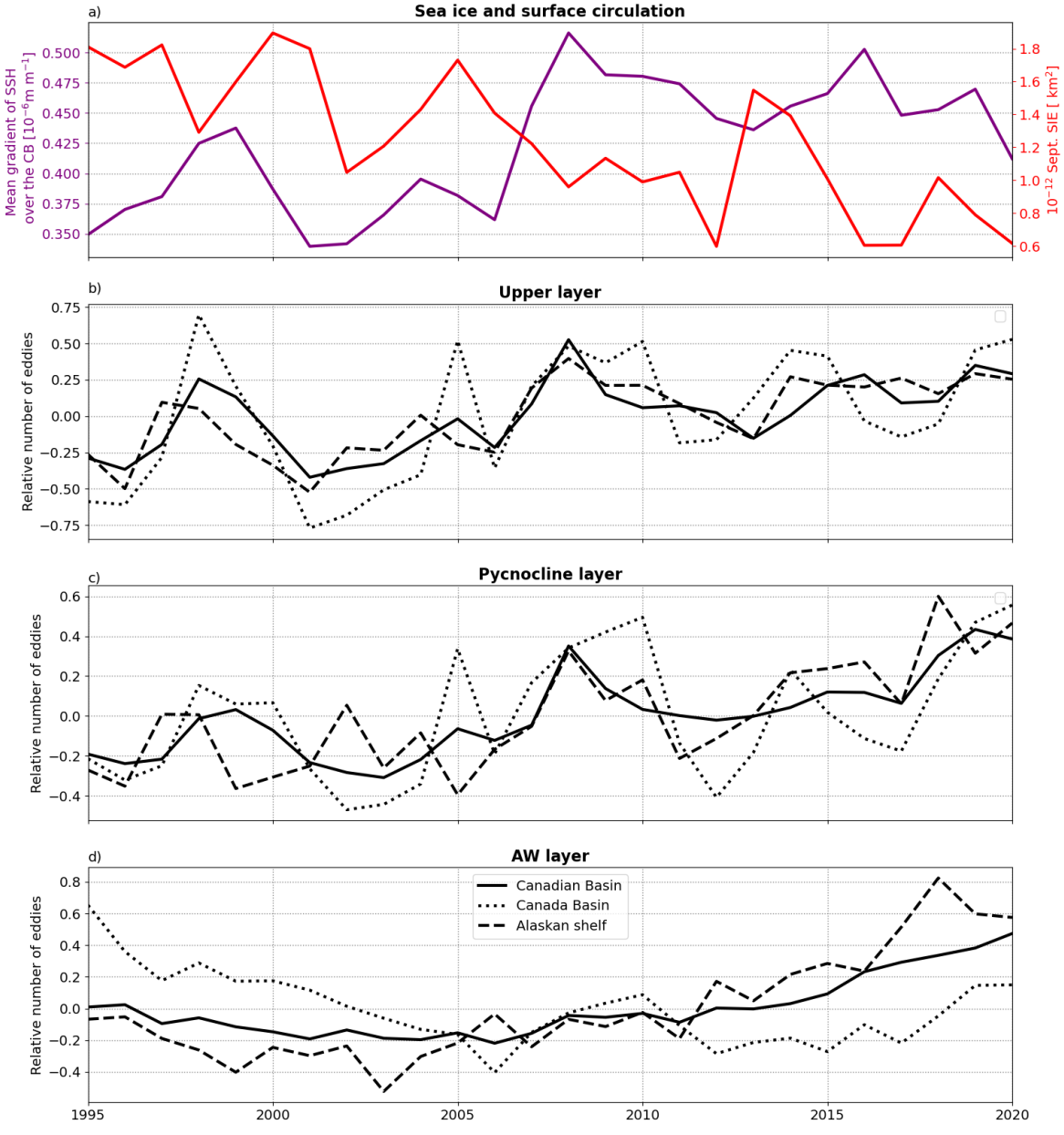

Figure 7. Time series of (a) the September sea ice extent over the Canadian Basin (red, total area of the domain is $2.7 \cdot 10^{12}$ km^2) and the gradient of SSH averaged over the CB (similar to the maximum SSH over the gyre, not shown). (b), (c) and (d) show the layer-averaged number of individual eddies detected relative to the 26-year average within that layer for (b) the upper layer, (c) the pycnocline layer, and (d) the AW layer for the whole Canadian Basin (plain black line), the Alaskan shelf area (dashed black line) and the Canada Basin (dashed dotted line).

https://doi.org/10.5194/egusphere-2025-3527
Preprint. Discussion started: 30 July 2025

the southern edge of the BG (Fig. 8a). There, a strong reduction in the number of eddies detected is found compared to the shelf and deep basin (Fig. 8a). This reduced eddy production compared to the upper layer occurs despite the eddies' relatively strong intensity, long duration and associated distance travelled along the anticyclonic flow (Fig. 8c,e,f). We suggest this local reduction in eddy generation to be linked to a stabilizing effect of the continental slope. The growth of instabilities is known to be hampered over regions where the ratio of the continental slope to the isopycnal slopes is greater than 1 (Manucharyan and Isachsen, 2019), as is the case for the slope of the CB in the model (Regan et al., 2020).

3.3.3 Decadal and interannual variability of eddy generation

Over 1995-2020, the number of individual eddies detected between the two pycnoclines shows a larger increase than in the upper layer ($+45\%$ *vs* $+34\%$, Fig. 7b,c). Regionally, increases in the number of eddies are also found in the CB ($+33\%$), and along the Alaskan coastline ($+70\%$) as well as for short-lasting ($+42\%$) and long-lasting ($+75\%$) eddies (classified by comparing their turnaround time scale to their duration, see Fig. E2). The relative number of eddies generated in the pycnocline layer shows important interannual variability, with similar variations as the upper layer, despite no significant correlations with the ice cover. In details, a strong increase in the number of eddies detected starts around the year 2000 and peaks around 2008 ($+54\%$ between 2006 and 2008, Fig. 7b,c). Concurrently, a fast accelerating period for the BG mean flow has been observed (Giles, 2012; Regan et al., 2019) and modelled (Regan et al., 2020) around 2007, and is also visible in CREG12 between 2005 and 2007 through the mean gradients of SSH averaged over the CB on Fig. 7a. The observed increase in the number of eddies that peaks in 2008 bears similarity to the EKE increase that was reported over one year by Regan et al. (2020) following the gyre acceleration in 2007. While similar interannual variability is visible in the Alaskan shelf area, the CB, however, display a strong increase in eddy generation around 2008 that persists for a couple of years beyond the peak in the BG intensity. The processes sustaining this high level of eddy generation beyond 2008 remain to be explored. The increase in the number of eddies at the end of the time period ($+46\%$ between 2012 and 2020) associated with a decrease in the gyre's intensity remains unexplained as a few more years of simulation would be necessary to conclude robustly about any trend and sustained changes.

3.4 Characteristics of eddies in the AW layer

3.4.1 Mean annual and seasonal eddy characteristics

Below the second pycnocline and down to 1,200 m, that is within the AW layer, the total number of eddies over the 26 years of simulation decreases by 37% compared to the pycnocline layer (from 8,900 to 5,600 eddies per year per depth level, Fig. 5a). Because the layer is located below the upper and lower pycnoclines, the seasonality in eddy properties is almost completely shut down (Fig. 5). In that layer, we find eddies with similar radius (≈ 11.8 km, Fig. 5b) but weaker than in the pycnocline layer ($1.5 \cdot 10^{-6}$ s^{-1} compared to $3.3 \cdot 10^{-6} s^{-1}$, Fig. 5c). The distance travelled by eddies decreases from 12.2 km to 7 km (Fig. 5f), and the polarity remains $\approx 50\%$ (Fig. 5d). We note that the average duration of eddies is larger than in the pycnocline layer (14 days compared to 11 days) but remains small considering the few processes that could dissipate eddies at this depth. This relatively short duration may point to the fact that most of the eddies detected in this layer are not well-developed and hence

https://doi.org/10.5194/egusphere-2025-3527
Preprint. Discussion started: 30 July 2025

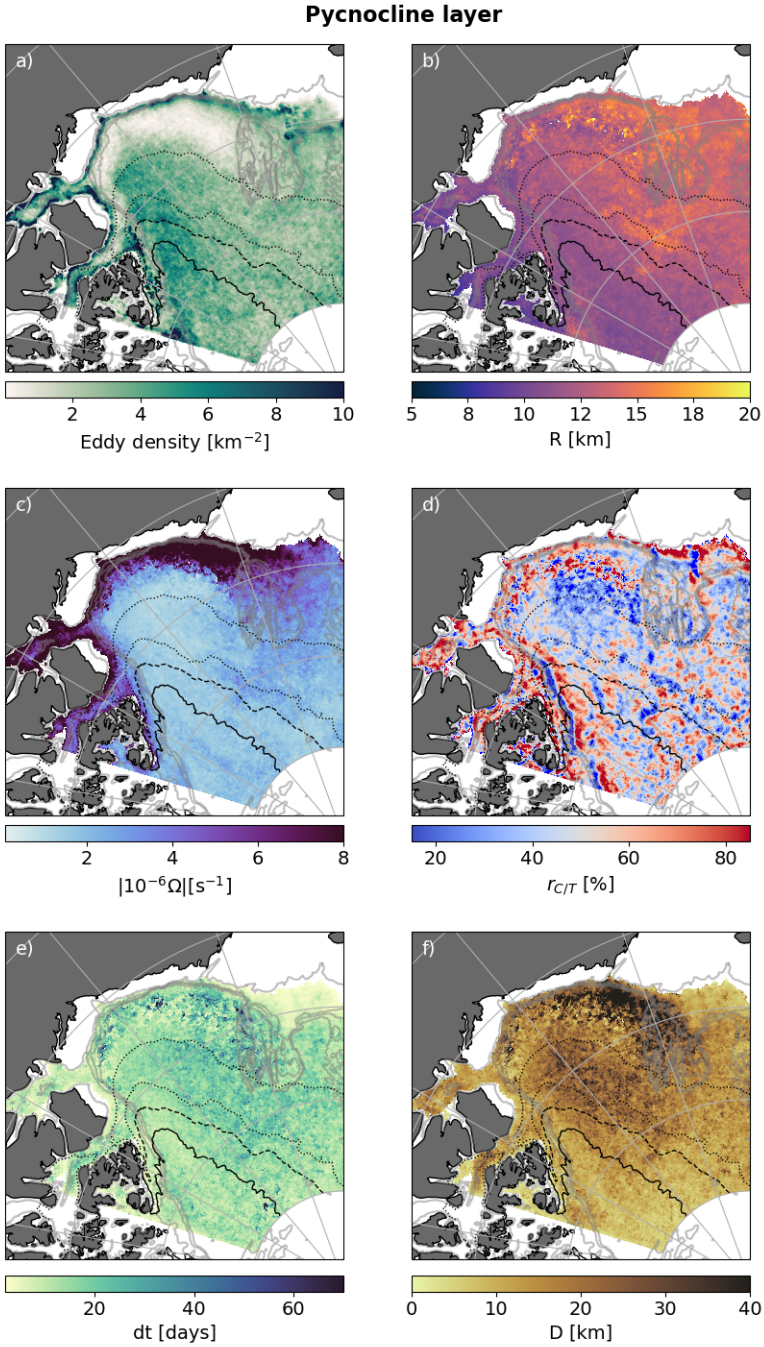

Figure 8. Eddy properties in the pycnocline layer (at 150 m) over the 26 years of simulation. (a) Eddy generation density (i.e. number of individual eddies detected per km^2) and associated properties: (b) averaged radius, (c) intensity, (d) polarity, (e) duration and (f) distance travelled. All variables are extracted at nominal depth 150 m, and averaged/summed over the 26 years of simulation. Note that all fields show similar structures at all depths between 85 and 225 m (see Fig. 5c). Plain, dashed, dotted and loosely dotted black lines show respectively the 90%, 80%,50% and 15% contours of the climatological September sea ice concentration. Gray shaded plain lines show the 100, 500, 1000, 1500 m isobaths.

https://doi.org/10.5194/egusphere-2025-3527
Preprint. Discussion started: 30 July 2025

bound to disappear quickly. Of all the eddies detected in that layer, 6% are well-developed so that they persist for longer than their turnaround time. These long lasting eddies may live up to 150 days (99^{th} percentile), which surpasses all the maximum durations detected in the other layer (see Sect. 4 for a discussion on the long-lasting eddies).

3.4.2 Spatial distribution of eddy characteristics

Within the AW layer, eddy properties show different patterns compared to the layers above. Significant differences are expected given that the mean geostrophic circulation of that layer departs strongly from that above (Fig. A1). In particular, eddies are predominantly generated over the continental slope along the path of the cyclonic boundary current carrying AW (Fig. 9a). Along these boundary currents, the eddy intensity is larger by up to one order of magnitude compared to the rest of the domain (Fig. 9c). Weaker eddies are generated throughout the rest of the domain but at a smaller generation rate ($4-8$ eddies per km^2 compared to $8-12$ eddies per km^2 along the slope). Along the shelf breaks of the Chukchi Sea and Canadian Archipelago, polarity show anticyclones dominating in the inshore part of the current and cyclones dominating in the offshore part of the current (Fig. 9d). Off the western flank of Northwind Ridge are found the largest, farthest-reaching and longest-lived eddies, with averaged radii as large as 20 km, travelled distances up to 40 km, and durations as long as 60 days (Fig. 9b,e,f). Large uncertainties exist on the exact path of the AW in this region where AW is thought to intermittently detach from the slope-intensified cyclonic boundary current and/or form double boundary currents (McLaughlin et al., 2009; Li et al., 2020; Planat et al., 2024; Karcher et al., 2012; Lique et al., 2015). In our model, the EKE is one order of magnitude larger in that area than within the deep basin and displays hotspots in the form of large structures detaching from the cyclonic boundary current hugging Northwind Ridge (not shown), that likely generate the large eddies detected. Finally, most hot spots in eddy density located close to the Northern boundary of our domain are associated to short-lived eddies, and the larger eddy density is likely a signature of the limitation of the detection algorithm with respect to very weak eddies that get lost over consecutive days.

3.4.3 Decadal and interannual variability of eddy generation

Similar to the pycnocline and surface layer, the AW layer shows a sustained increase in the number of eddies generated over the 26 years of about $+40\%$ in the Canadian Basin (Fig. 7d). The Alaskan shelf area shows an increase of $+92\%$ while in contrast, the Canada Basin shows an overall decrease (-26%). However, the increase at the end of the time series for the CB ($+59\%$ between 2015 and 2020) suggests a lagged increase that cannot be seen due to the length of the time series. In contrast to the layers above, little interannual variability is visible on top of the overall increase in eddy generation. This is also true for the short-lasting eddies, that represent the vast majority of the population within that layer, but not for the long-lasting eddies, that only represent 6% of the total population and display important year-to-year variability. These more persistent features show a large relative increase ($+300\%$) starting around 2011 (see Fig. E2). This is mostly an increase in the number of large eddies located east of NWR that are possibly associated with the cyclonic boundary current detaching from the bathymetry. These large structures occur in particular in the late years of the simulation (2012-2020) when the cyclonic flow on the north-western flank of Northwind Ridge reverses to an anticyclonic flow with increased shear (not shown). What drive these changes in the AW mean and eddy circulations and how they influence the generation of large eddies is beyond the scope of this

https://doi.org/10.5194/egusphere-2025-3527
Preprint. Discussion started: 30 July 2025

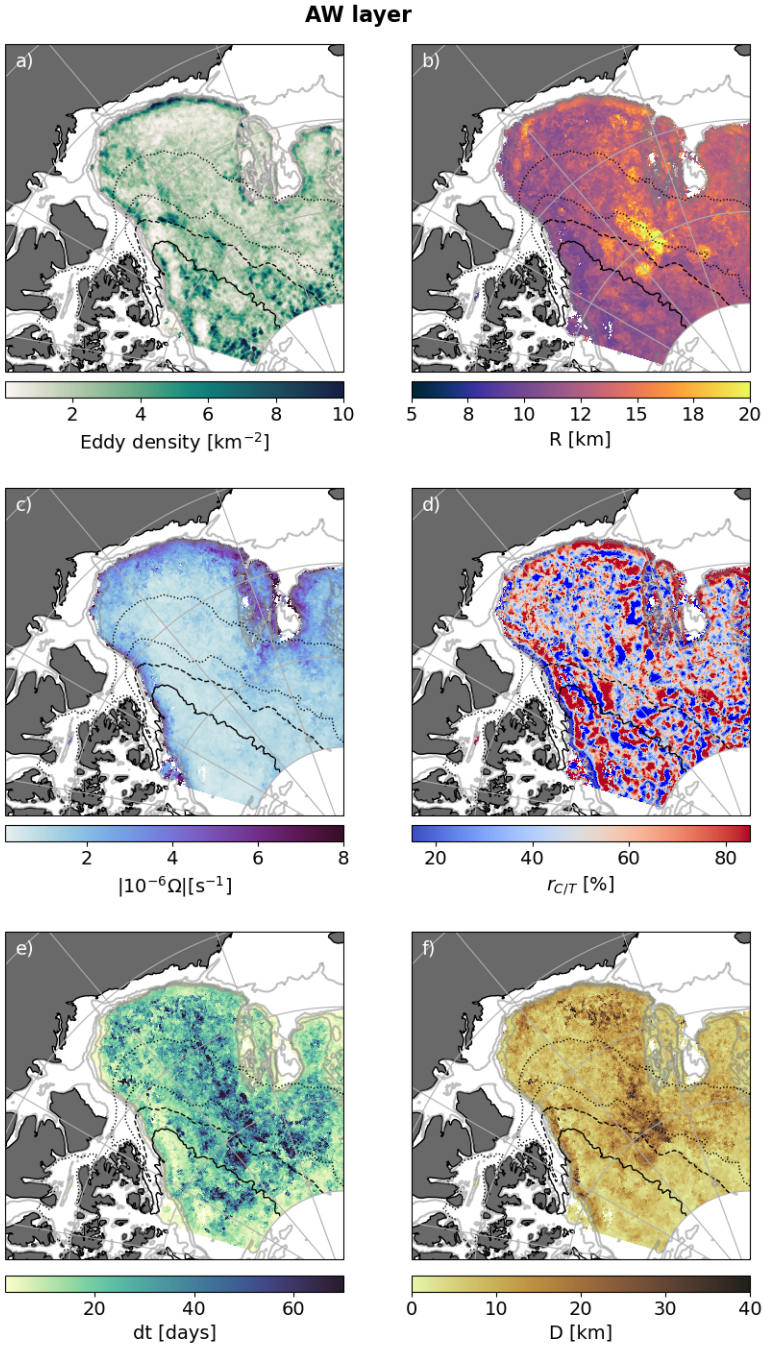

Figure 9. Eddy properties in the AW layer (at 500 m) over the 26 years of simulation. (a) Eddy generation density (i.e. number of individual eddies detected per km^2) and associated properties: (b) averaged radius, (c) intensity, (d) polarity, (e) duration and (f) distance travelled. All variables are extracted at nominal depth 500 m, and averaged/summed over the 26 years of simulation. Note that all fields show similar structures at all depths between 225 and 1200 m (see Fig. 5c). Plain, dashed, dotted and loosely dotted black lines show respectively the 90%, 80%,50% and 15% contours of the climatological September sea ice concentration. Gray shaded plain lines show the 100, 500, 1000, 1500 m isobaths.

https://doi.org/10.5194/egusphere-2025-3527
Preprint. Discussion started: 30 July 2025

paper and is left for future analysis. The number of eddies in the Canada Basin also exhibits some interannual variability, in particular showing a small but significant transient increase around 2007-2010 similar to the one described in the pycnocline layer associated with the acceleration of the Gyre. Such a direct top-down coupling between the Beaufort Gyre and the AW circulation was already documented by Lique and Johnson (2015); Lique et al. (2015) for the mean circulation of the AW layer. This more energetic mean flow may in turns generates more mesoscale eddies.

4 Discussion and conclusion

In this study, we apply an eddy detection and tracking algorithm to the output of a high-resolution regional model of the Arctic in order to document the characteristics of mesoscale eddies in the Canadian Basin. We report an average of 6,250 eddies generated per year and per model depth within the top 1,200 m of the Canadian Basin for the period 1995-2020. Most of these eddies are found to be the size of the Rossby radius of deformation (mean eddy radius about 12.1 km), stationary (distance travelled about 11.1 km) and short lasting (duration about 10 days; Fig. 4). The distribution between cyclones and anticyclones is about equal in the investigated domain. In addition, most eddies do not have a temperature nor salinity anomaly relative to their environment. All the documented properties (radius, polarity, intensity, duration, distance travelled and temperature and salinity anomaly) vary significantly across space and time (see Table 2), thus suggesting a variety of processes that generate and dissipate eddies in the stratified Canadian basin.

Our analysis highlights three layers within the Canadian Basin with consistent characteristics across the vertical. In the upper layer (top 85 m), which lies above the first pycnocline on average, eddy properties display a significant seasonal cycle generally in phase with that of sea ice. The largest generation rate for eddies occurs when sea ice concentration decreases below 80%, a threshold in line with the results of Manucharyan and Thompson (2022). At about $\sim$70 m, the first pycnocline insulates the eddy field from dissipation by sea ice. Therefore, weaker seasonality is detected in the eddy characteristics below this depth. However, interannual variability in the number of eddies related to changes in the large scale circulation can still be observed. Over 2007-2008, the BG acceleration likely leads to an increase in the number of eddies followed by a quick return to the pre-acceleration number in 2009, as suggested by Regan et al. (2020). An increase in number of eddies can be detected down to 1200 m in the CB, though it takes about 4 years to drop to pre-acceleration levels of eddy generation after 2008. The reasons of this slower decrease remains unexplained and deserves further investigation in future work. Apart for this transient increase in number of eddies in the CB, the AW layer show little to no similarities to the layers above, in line with the efficient insulation of the lower pycnocline. In particular, while the upper and pycnocline layers of the Canadian Basin show anticyclones forming preferably at the centre of the Beaufort Gyre, in the AW layer anticyclones are found in-shore and cyclones off-shore of the boundary current along the slope. Finally, it is important to note that the definition of the three layers relies on the statistical properties of the whole eddy field over 26 years and does not account for temporal variability of the mean circulation, the location of the gyre, and the mean isopycnal depths and slopes which additionally vary across the basin. Thus, the depths used as delimiters of the three layers do not necessarily correspond to the actual, instantaneous pycnoclines that they are assumed to represent at all times. Nevertheless, the results presented in this study, and in particular the spatial structure of the eddy prop-

https://doi.org/10.5194/egusphere-2025-3527
Preprint. Discussion started: 30 July 2025

	Nmb. of eddies		R [km]		dt [days]		D [km]		$r_{C/T}$ [%]		$\|\Omega\|$ [s^{-1}]		ΔT [°C]		ΔS [psu]	
Upper layer	6000	2.4	12.4	0.1	5.4	0.6	11.3	0.7	48.1	0.09	7.410^{-6}	0.4	0.08	1.7	-0.01	-7.1
Pycnocline layer	8900	0.6	11.6	0.04	10.8	0.1	12.2	0.3	49.5	0.05	3.310^{-6}	0.3	0.01	5.1	0.008	6.3
AW layer	5600	0.5	11.8	0.02	14.2	0.3	7.1	0.1	50.8	0.06	1.510^{-6}	0.2	0.003	1.1	-0.003	-2.5
Total	6250	2.6	12.1	0.06	9.9	0.2	11.1	0.4	49	0.05	4.610^{-6}	0.04	0.04	1.6	-0.006	7.6

Table 2. Mean (left) and seasonal cycle amplitudes (right) of the eddy properties reported along this manuscript for each layer and for the Canadian Basin as a whole.

erties and their temporal variability, remain consistent when slightly varying the layers' upper and lower boundaries indicating the robustness of the key features reported for the three layers.

Of particular interest when comparing to our 50-50 ratio of cyclones and anticyclones is the ratio of 95% anticyclones exhibited by the ITP dataset (Cassianides et al., 2023; Zhao et al., 2014), although one should keep in mind that this dataset contains primarily sub-mesoscale features. Even more surprising, the symmetry remains valid if we subsample the dataset to only account for small eddies ($R < 15$ km) that are more likely to resemble the submesoscale coherent vortices detected from the ITP dataset. The predominance of anticyclones exhibited by the ITP dataset concerns the centre of the BG which is where ITPs are mainly deployed due to the sea ice being the thickest (see App. F1 for details). A vertical asymmetry with the formation of dipoles of cyclones at the surface and anticyclones subducting within the pycnocline was suggested to explain the asymmetry observed in the ITP dataset (Manucharyan and Timmermans, 2013). A similar asymmetry was suggested in the Southern Ocean to explain the predominance of cyclones observed at the surface in the MIZ (Auger et al., 2023). In our model, the centre of the BG does display a larger proportion of anticyclones than cyclones (Figures 6d, and 8d) but no evidence of such vertical structure appears. More specifically, when applying our eddy detection following the temporal and spatial sampling of the ITPs, we find a proportion of anticyclones that increases on average from 51% to 65% in our model. Though the comparison with the ITP dataset is somewhat limited by the fact that the observed eddy field may be dominated by sub-mesoscale features, which our model does not resolve, our results suggest that part of the anticyclonic dominance documented by the ITP dataset is linked to the ITP sampling location, as was already suggested by Beech et al. (2025). Due to the limits of both the detection algorithm and the model's ability to resolve the smaller Rossby radius and associated mesoscale instabilities over the shelf, we cannot extend this analysis to the satellite sampling area that mostly covers Northwind Ridge and the Chukchi shelf (see Figure 2 from Kozlov et al., 2019). Still, we do observe a higher ratio of cyclones along the edges of the gyre (Figure 6d) and suggest it could correspond to the dominance of cyclones over anticyclones documented in Kozlov et al. (2019).

Our algorithm identifies as "eddy" a broad range of features, from the ephemeral ones that last a couple of days to the more persistent ones that are likely more coherent. When separating between short and long-lasting eddies based on their duration being respectively shorter or longer than their turnaround time, we find that the bulk of the eddy dataset consists of short-lasting eddies. The ephemeral eddy population that our study detects is likely not represented in observational dataset which

https://doi.org/10.5194/egusphere-2025-3527
Preprint. Discussion started: 30 July 2025

may explain some of the important differences found with the literature based on observations. Yet, these eddies may play an important role in the transfer of energy.

Long-lasting eddies may resemble more the eddy population captured by observations. We find that these eddies represent 15% of the population in the upper layer, 10% in the pycnocline layer and 6% in the AW layer (see also the mean statistical properties of long-lasting eddies in Appendix E1). A fraction of these eddies display temperature anomalies, in particular along the shelf break. These anomalies are mostly positive at the surface where they are formed either within the mixed layer or the warm Near Surface Temperature Maximum; and in the upper part of the pycnocline layer, where they form within the warm summer Pacific Waters. In contrast, these anomalies are mostly negative in the lower part of the pycnocline layer where they form in the cold winter Pacific Waters. Note that because these long-lasting eddies are mostly generated in regions of intense eddy generation, such as Pt. Barrow, the environment surrounding these eddies has strong temperature gradients and thus the anomalies do not meet the "significant" criteria - despite the anomaly being clearly visible (see Fig. 10). Still, because these long-lasting eddies travel for a few tens of kilometres, we hypothesize that the most coherent eddies actively play a role in transporting heat, in line with previous observations of warm eddies directly penetrating into the CB from Point Barrow (MacKinnon et al., 2021). One example of such an eddy is given on Fig. 10a, with an anticyclone carrying warm water off-shore when leaving Pt Barrow. This eddy is seen to subduct at depth from mi-September, with a colder and fresher layer developing above (Fig. 10b). However, a robust quantification of the heat transport associated with these eddies is not trivial as it requires computing the temperature anomaly which is highly dependent upon the definition of the environment. This analysis is thus left for future work.

To conclude, we present a first characterization of the spatio-temporal properties of mesoscale eddies in the Canadian Basin. By doing so, we unraveled strong differences in eddy properties across the basin and seasons, as well as important variability in the number of eddies generated over 1995-2020. By providing a thorough characterization of eddy properties in the Canada Basin, this model-based eddy census can inform the analyses and interpretation of eddy censuses based on observations and help quantify some of the biases associated to in-situ deployments. Furthermore, our dataset could form a starting point to explore questions that remain on the BG dynamical and thermodynamical equilibrium, as well as on the transport and stirring of nutrients, salt, or other tracers. In particular, future work could include an analysis of the interannual to decadal evolution of the eddy properties to help investigate their possible future effects on the environment through transport and stirring of nutrients, salt, or other tracers as sea ice retreats and the BG gets more energetic.

Code and data availability. The *eddytools* python package used to perform the eddy detection and tracking along with its documentation is available at https://github.com/jk-rieck/eddytools@N-tracking-properties. The scripts used in this study to detect, track and analyse the mesoscale eddies are available at https://github.com/noemieplanat/Eddies_CB/releases/tag/submission. The documentation of the CREG12 experiment can be found in Talandier and Lique (2024). The eddy dataset is available upon request.

https://doi.org/10.5194/egusphere-2025-3527
Preprint. Discussion started: 30 July 2025

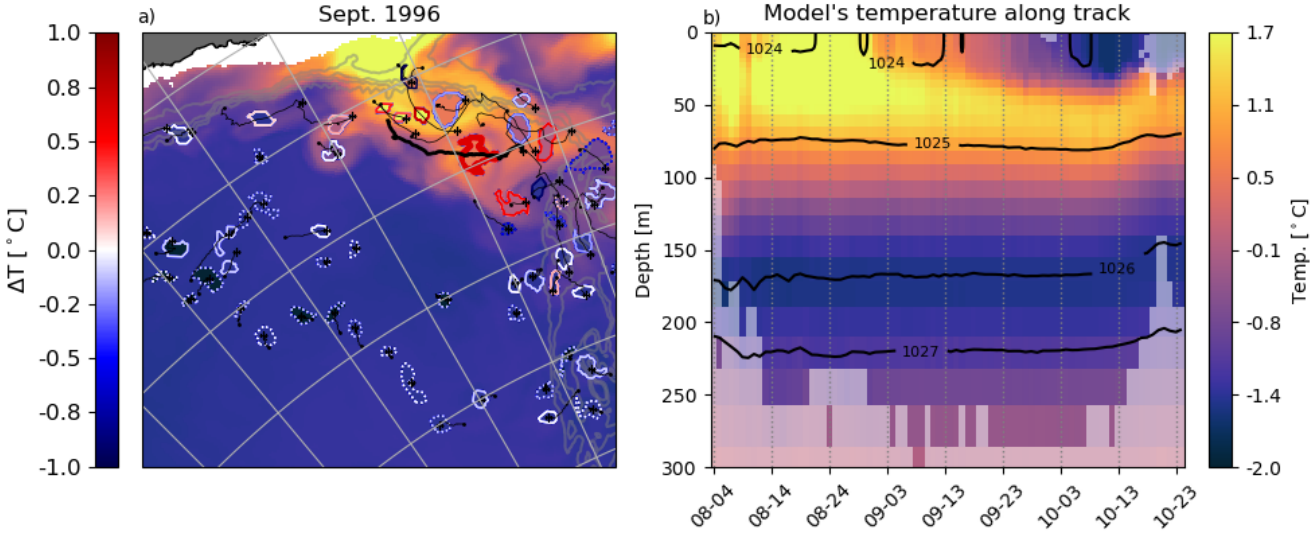

Figure 10. (a) Conservative Temperature at 30 m in September 1996 overlaid with all long-lasting eddies detected (and not necessarily born) on September 16th 1996. Coloured contours indicate the temperature anomaly of eddies, thin black lines their trajectory. Eddies are colored by their mean temperature. (b) Model temperature along the eddy track identified on (a) with a thicker black line. At a given depth, intense color shading indicates that the algorithm detects an eddy at that depth, location and time while pale color shading indicates that no eddy is detected. Thick black lines show isopycnals along the eddy track.

https://doi.org/10.5194/egusphere-2025-3527
Preprint. Discussion started: 30 July 2025

Author contributions. NP designed and conducted the study with input from COD, CL and LBT. CT and CL ran CREG12 model. JKR built the eddytools python package and NP applied it on the output of CREG12 with appropriate modifications. NP processed and analyzed the eddy database. NP, JKR, COD, CL and LBT contributed to the interpretation. NP wrote the manuscript, with contribution from COD, CL, LBT, JKR and CT for editing.

Competing interests. The authors declare no conflict of interest.

Acknowledgements. NP was supported by the Fonds de recherche du Québec - Nature et Technologie (FRQNT) through a Doctoral Training Scholarship, a Natural Sciences and Engineering Research Council of Canada (NSERC) Accelerator Supplements awarded to COD (grant no. RGPAS/2018-522502), and a NSERC Discovery Grant awarded to BT (grant no. RGPIN/2018-04838). NP also received a scholarship from ISblue (Interdisciplinary graduate school for the blue planet - ANR-17-EURE-0015) and financial support from Québec-Océan for this work. COD and JKR acknowledge funding from NSERC through the Accelerator Supplements (grant no. RGPAS/2018-522502) and a Canada Research Chair (grant no. 252794), both awarded to COD. NP, COD, CL, JKR and LBT acknowledge the financial support from the Fonds de recherche du Québec – Nature et technologies (FRQNT) and the French Ministry of Europe and Foreign Affairs through the Samuel-de-Champlain grant (https://doi.org/10.69777/329860). CL and CT were supported by funding from the CLIMArcTIC project funded by the "PPR Océan et Climat—France 2030" (contract ANR-22-POCE-0005). The pan-Arctic simulations were performed using HPC resources from the French GENCI-CINES center (Grant 2023-A0130107420). The authors also acknowledge the technical and scientific contributions of Benjamin Valette and Sacha Coez to the preparatory phase of the study.

Appendix A: Mean Kinetic Energy from CREG12 and from mooring estimates of von Appen et al. (2022)

Appendix B: Sensitivity to method's parameters α

Appendix C: Changes of eddy properties simultaneously along 2 properties

Appendix D: Seasonal changes comparatively along the coast and off shore

Appendix E: Long-eddies characteristics

Appendix F: Spatial repartition of ITPs across the CB between 2003 and 2024

We compute an occupation ratio for the ITP dataset on an Equal-Area Scalable Earth grid of 25 km large. We include all ITPs processed to level-3 of post-processing between 2003 and 2024 (Toole et al., 2011) and the profiles are binned per day. The occupation is computed for each grid cell, as the number of profiles by the total number of profiles (Fig. F1).

https://doi.org/10.5194/egusphere-2025-3527
Preprint. Discussion started: 30 July 2025

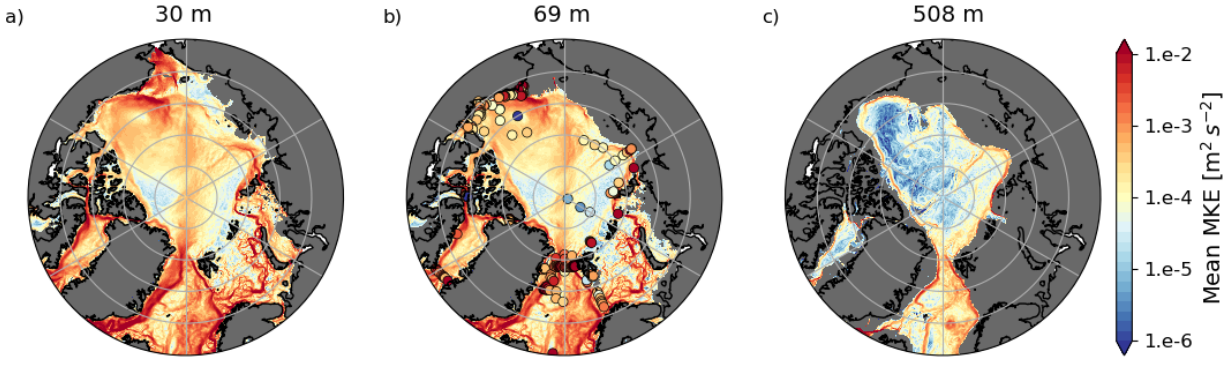

Figure A1. Mean Kinetic Energy (MKE) computed from monthly averages and averaged over the 26 years of simulation (a) within the surface layer at 30 m, (b) within the halocline at 69 m and (c) within the AW layer at 508 m. Super-imposed on (b) are mooring estimates of MKE from von Appen et al. (2022) computed for depths between 50-100 m, corresponding to monthly deviations, please refer to this paper for exact calculation methodology.

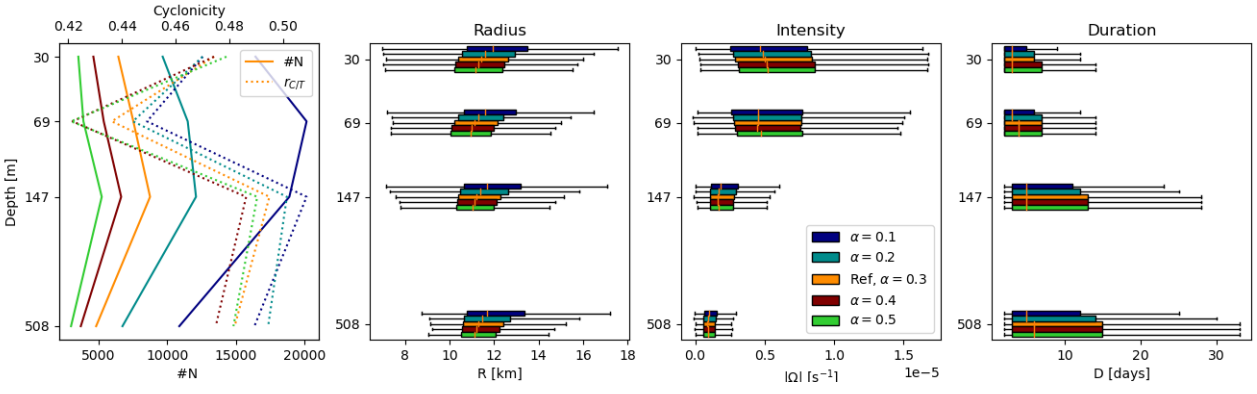

Figure B1. (a) polarity (dotted lines) and number of eddies detected (plain lines); median and 90/10-th percentiles for (b) the radius, (c) the intensity (absolute value of vorticity Ω) and (d) the duration when varying the detection parameter α from 0.2 to 0.5. Sensibility is assessed at 35 m, 69 m, 120 m, 200 m and 550 m for one year (chosen randomly as 2001) and for the whole Canadian Basin.

Appendix G: Time series of eddy generation for the different sea ice concentration (sic) categories: Open Ocean (sic $< 0.15\%$), MIZ ($0.15\% <$sic$< 0.8\%$) and Pack ice (sic$> 0.8\%$)

https://doi.org/10.5194/egusphere-2025-3527
Preprint. Discussion started: 30 July 2025

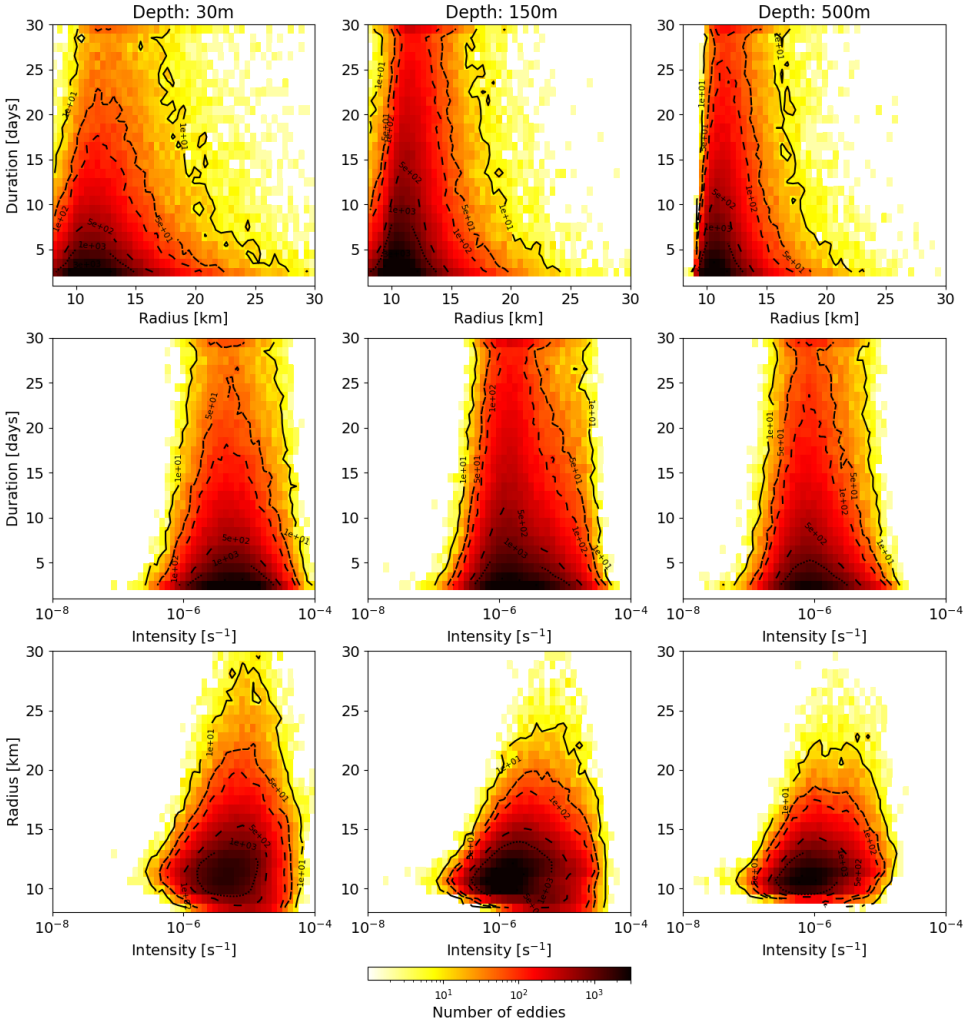

Figure C1. Histogram of duration, intensity and radius simultaneously at 30 m (first column), 150 m (second column) and 500 m (last column). First row display duration *vs* radius, second row duration *vs* intensity and last row radius *vs* intensity. Plain, dashed, loosely dashed, very loosely dashed and dotted lines indicate iso-contours of 10, 50, 100, 500 and 1000 eddies.

https://doi.org/10.5194/egusphere-2025-3527
Preprint. Discussion started: 30 July 2025

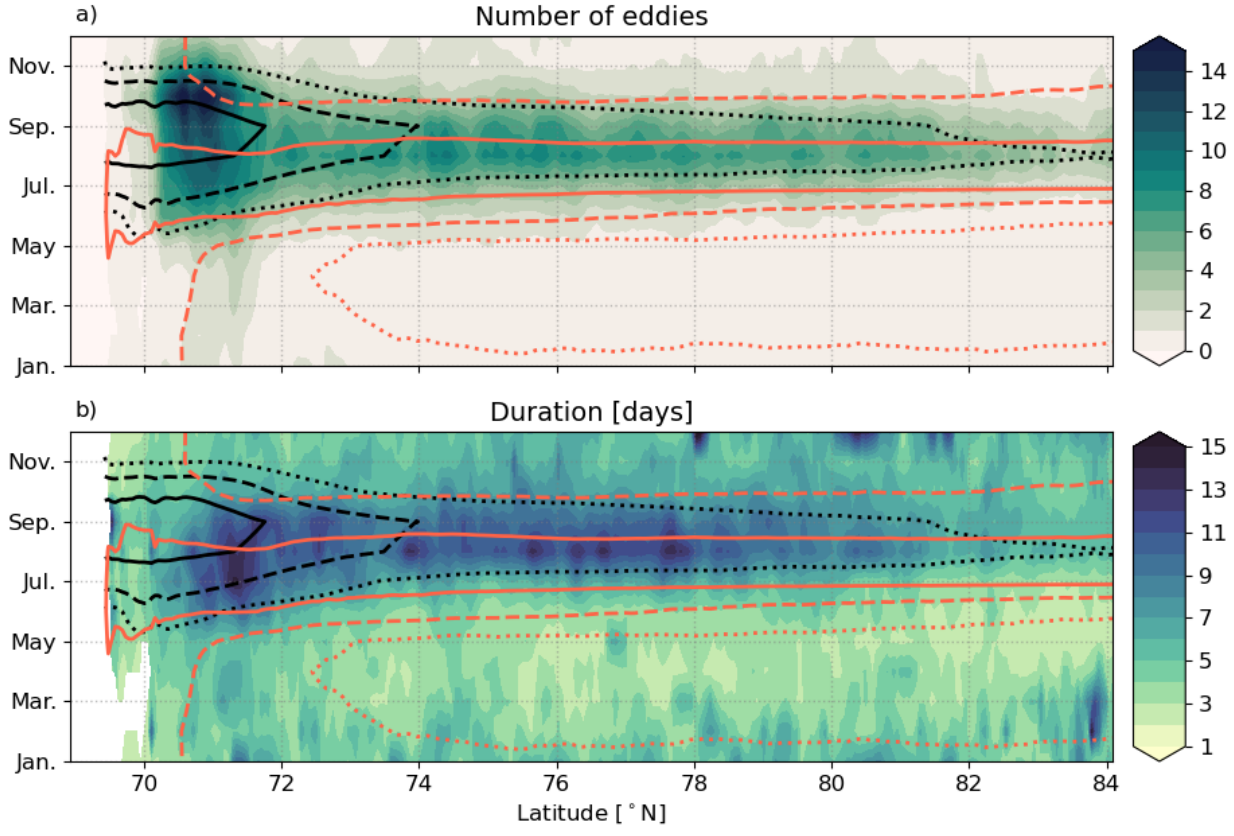

Figure D1. Hovmöller diagram of a latitudinal section from the Alaskan shelf to the center of the Arctic (see red line on Fig. 1) against seasons for (a) the total number of eddies detected over the 26 years and (b) eddy duration. Both fields are summed or averaged zonally across a band of 150 km and vertically averaged within the upper layer (from surface to 85 m). Black plain, dashed and dotted lines indicate the 0.15, 0.5 and 0.8 sea ice fraction. Orange plain, dashed and dotted lines indicate the 5 m, 20 m and 40 m mixed layer depth.

https://doi.org/10.5194/egusphere-2025-3527
Preprint. Discussion started: 30 July 2025

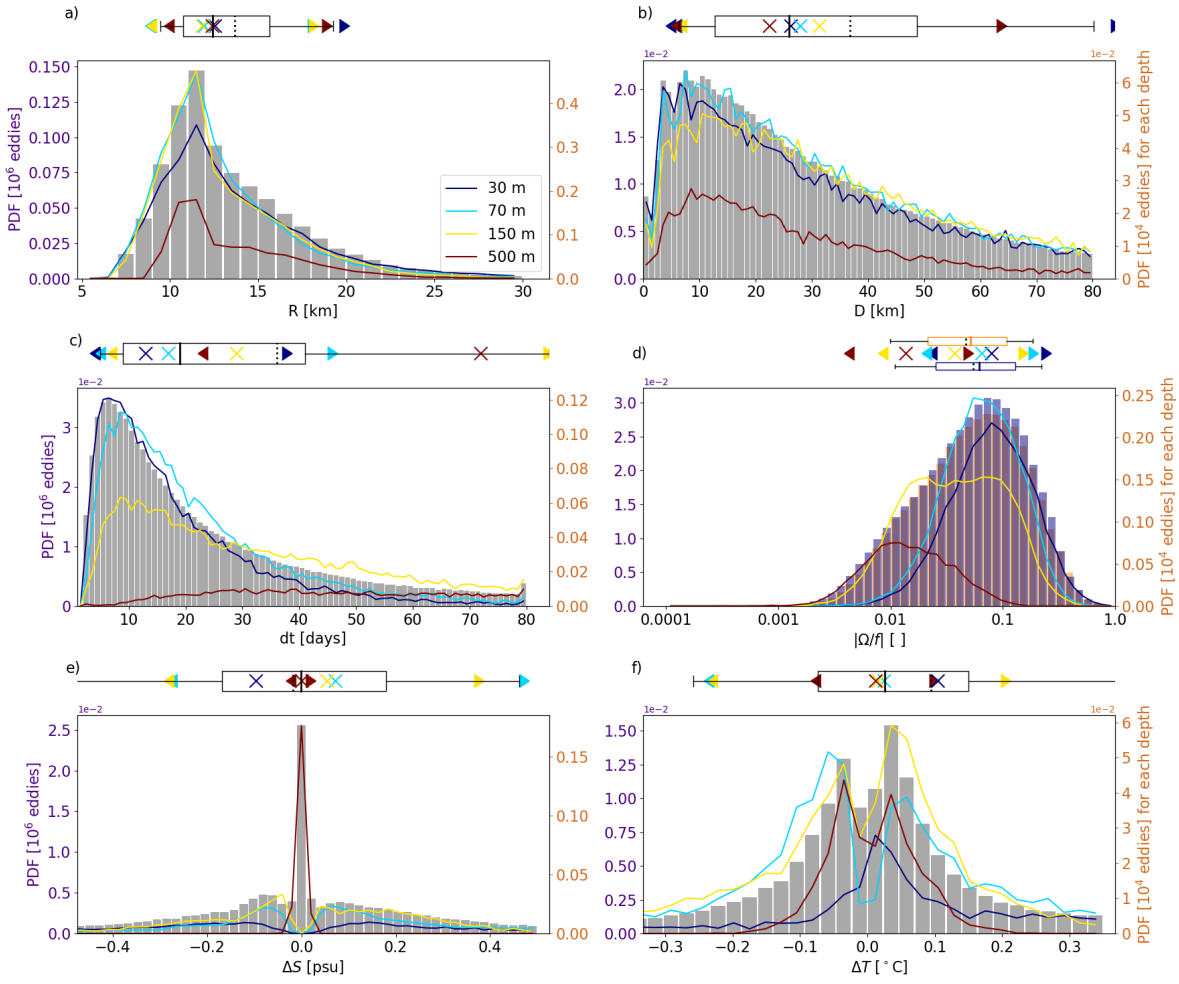

Figure E1. Same as Fig. 4 for long-lived eddies only

https://doi.org/10.5194/egusphere-2025-3527
Preprint. Discussion started: 30 July 2025

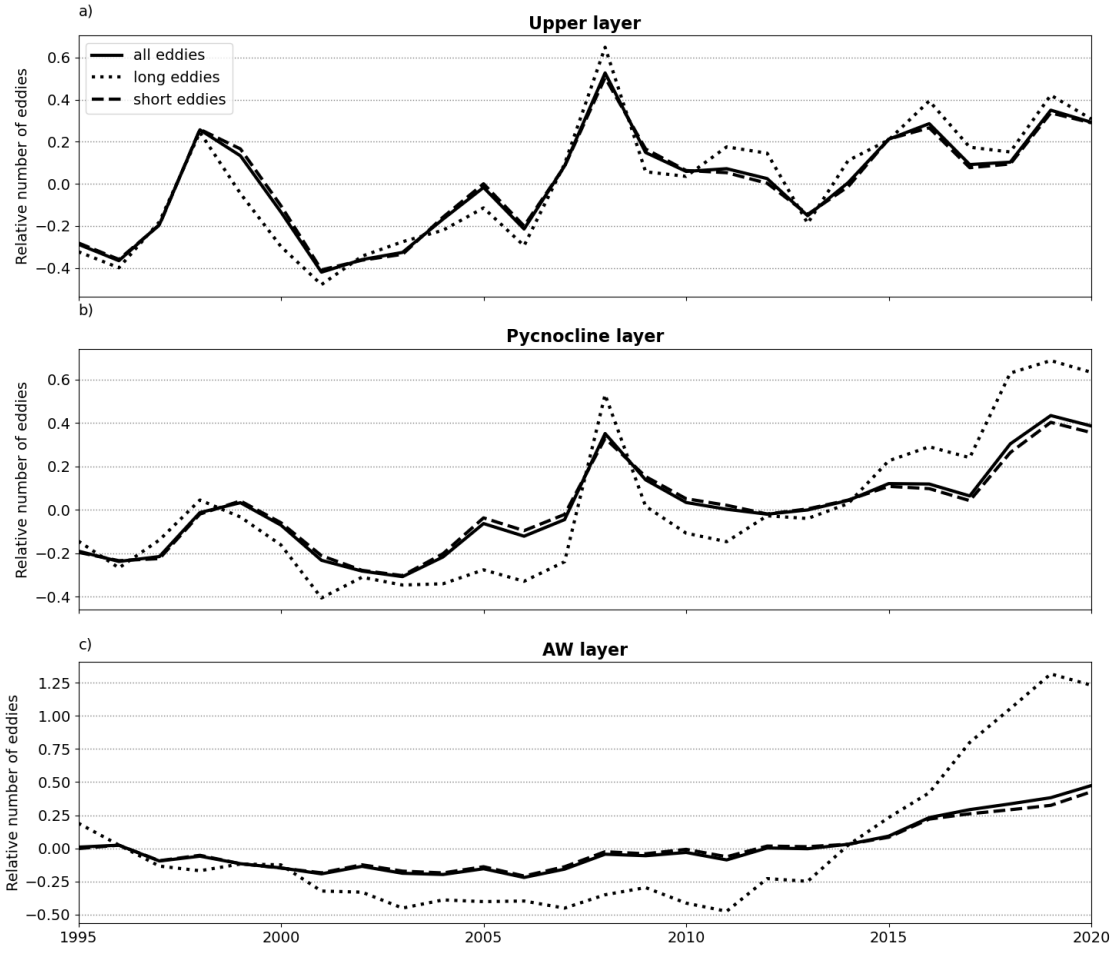

Figure E2. Time series of the relative number of eddies generated within the Canadian Basin for (a) the upper layer, (b) the pycnocline layer and (c) the AW layer, for respectively the short eddies (dashed lines), long eddies (dotted lines) and for all eddies (plain lines, identical to Fig. 7).

https://doi.org/10.5194/egusphere-2025-3527
Preprint. Discussion started: 30 July 2025

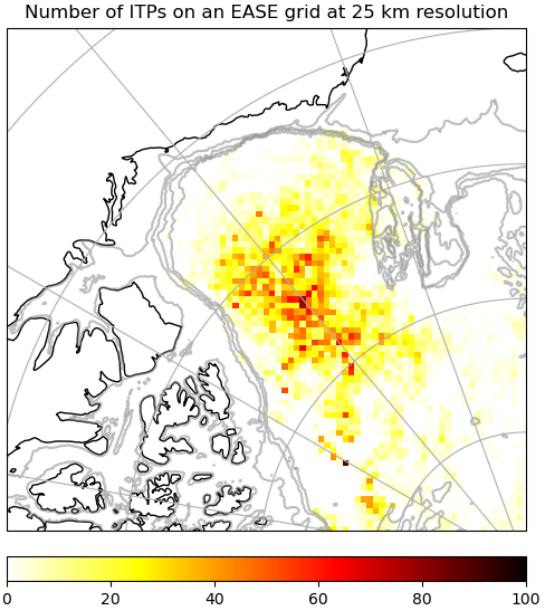

Figure F1. Number of ITP profiles available per Equal-Area Scalable Earth grid cell for an EASE grid of 25 km large. All ITPs processed to level-3 of post-processing between 2003 and 2024 are included and binned per day (Toole et al., 2011).

https://doi.org/10.5194/egusphere-2025-3527
Preprint. Discussion started: 30 July 2025

Figure G1. Time series of the relative number of eddies generated within the Canadian Basin in the upper layer for the three sea ice regions : Open Ocean (dashed lines), MIZ (dash-dotted lines) and Pack ice (dotted lines). The time series are weighted (b, respectively not weighted on panel a) by the yearly cumulated ice area of each region.

https://doi.org/10.5194/egusphere-2025-3527
Preprint. Discussion started: 30 July 2025

References

Antonov, J. I., Seidov, D., Boyer, T. P., Locarnini, R. A., Mishonov, A. V., Garcia, H. E., Baranova, O. K., Zweng, M. M., and Johnson, D. R.: World Ocean Atlas 2009, Volume 2: Salinity., Tech. rep., U.S. Government Printing Office, Washington, D.C., 2010.

Armitage, T. W. K., Bacon, S., Ridout, A. L., Thomas, S. F., Aksenov, Y., and Wingham, D. J.: Arctic sea surface height variability and change from satellite radar altimetry and GRACE, 2003–2014, Journal of Geophysical Research, [Dataset]http://www.cpom.ucl.ac.uk/dynamic_topography/, 2016.

Armitage, T. W. K., Manucharyan, G. E., Petty, A. A., Kwok, R., and Thompson, A. F.: Enhanced eddy activity in the Beaufort Gyre in response to sea ice loss, Nature Communications, 11, 761, https://doi.org/10.1038/s41467-020-14449-z, 2020.

Auger, M., Sallée, J., Thompson, A. F., Pauthenet, E., and Prandi, P.: Southern Ocean Ice-Covered Eddy Properties From Satellite Altimetry, Journal of Geophysical Research: Oceans, 128, e2022JC019 363, https://doi.org/10.1029/2022JC019363, 2023.

Barnier, B., Blaker, A., Biastoch, A., Boening, C., Coward, A. C., Deshayes, J., Duchez, A., Hirschi, J., Sommer, J. L., Madec, G., Maze, G., Molines, J. M., New, A., Penduff, T., Scheinert, M., Talandier, C., and Treguier, A. M.: DRAKKAR:develop ing high resolution ocean components for European Earth system models, 2014.

Barton, B. I., Lique, C., Lenn, Y., and Talandier, C.: An Ice-Ocean Model Study of the Mid-2000s Regime Change in the Barents Sea, Journal of Geophysical Research: Oceans, 127, e2021JC018 280, https://doi.org/10.1029/2021JC018280, 2022.

Beech, N., Rackow, T., Semmler, T., and Jung, T.: High-latitude Southern Ocean eddy activity projected to evolve with anthropogenic climate change, Communications Earth & Environment, 6, https://doi.org/10.1038/s43247-025-02221-4, publisher: Springer Science and Business Media LLC, 2025.

Cassianides, A., Lique, C., Tréguier, A., Meneghello, G., and De Marez, C.: Observed Spatio-Temporal Variability of the Eddy-Sea Ice Interactions in the Arctic Basin, Journal of Geophysical Research: Oceans, 128, e2022JC019 469, https://doi.org/10.1029/2022JC019469, 2023.

Cavalieri, D. J., Gloersen, P., and Campbell, W. J.: Determination of sea ice parameters with the NIMBUS 7 SMMR, Journal of Geophysical Research: Atmospheres, 89, 5355–5369, https://doi.org/10.1029/JD089iD04p05355, 1984.

Chelton, D. B., Schlax, M. G., Samelson, R. M., and De Szoeke, R. A.: Global observations of large oceanic eddies, Geophysical Research Letters, 34, 2007GL030 812, https://doi.org/10.1029/2007GL030812, 2007.

Comiso, J. C.: Characteristics of Arctic winter sea ice from satellite multispectral microwave observations, Journal of Geophysical Research, 91, 975, https://doi.org/10.1029/JC091iC01p00975, 1986.

Corlett, W. B. and Pickart, R. S.: The Chukchi slope current, Progress in Oceanography, 153, 50–65, https://doi.org/10.1016/j.pocean.2017.04.005, 2017.

De Lavergne, C., Madec, G., Capet, X., Maze, G., and Roquet, F.: Getting to the bottom of the ocean, Nature Geoscience, 9, 857–858, https://doi.org/10.1038/ngeo2850, 2016.

DiGirolamo, N., Parkinson, C., Cavalieri, D., Gloersen, P., and Zwally, H.: Sea Ice Concentrations from Nimbus-7 SMMR and DMSP SSM/I-SSMIS Passive Microwave Data, https://doi.org/10.5067/MPYG15WAA4WX, 2022.

Dupont, F., Higginson, S., Bourdallé-Badie, R., Lu, Y., Roy, F., Smith, G. C., Lemieux, J.-F., Garric, G., and Davidson, F.: A high-resolution ocean and sea-ice modelling system for the Arctic and North Atlantic oceans, Geoscientific Model Development, 8, 1577–1594, https://doi.org/10.5194/gmd-8-1577-2015, 2015.

https://doi.org/10.5194/egusphere-2025-3527
Preprint. Discussion started: 30 July 2025

Giles, K. A.: Western Arctic Ocean freshwater storage increased by wind-driven spin-up of the Beaufort Gyre, NATURE GEOSCIENCE, 5, 2012.

Giulivi, C. F. and Gordon, A. L.: Isopycnal displacements within the Cape Basin thermocline as revealed by the Hydrographic Data Archive, Deep Sea Research Part I: Oceanographic Research Papers, 53, 1285–1300, https://doi.org/10.1016/j.dsr.2006.05.011, 2006.

Gupta, M., Gürcan, E., and Thompson, A. F.: Eddy-Induced Dispersion of Sea Ice Floes at the Marginal Ice Zone, Geophysical Research Letters, 51, e2023GL105 656, https://doi.org/10.1029/2023GL105656, 2024.

Hersbach, H., Bell, B., Berrisford, P., Hirahara, S., Horányi, A., Muñoz-Sabater, J., Nicolas, J., Peubey, C., Radu, R., Schepers, D., Simmons, A., Soci, C., Abdalla, S., Abellan, X., Balsamo, G., Bechtold, P., Biavati, G., Bidlot, J., Bonavita, M., De Chiara, G., Dahlgren, P., Dee, D., Diamantakis, M., Dragani, R., Flemming, J., Forbes, R., Fuentes, M., Geer, A., Haimberger, L., Healy, S., Hogan, R. J., Hólm, E., Janisková, M., Keeley, S., Laloyaux, P., Lopez, P., Lupu, C., Radnoti, G., De Rosnay, P., Rozum, I., Vamborg, F., Villaume, S., and Thépaut, J.: The ERA5 global reanalysis, Quarterly Journal of the Royal Meteorological Society, 146, 1999–2049, https://doi.org/10.1002/qj.3803, 2020.

Hu, X., Myers, P. G., and Lu, Y.: Pacific Water Pathway in the Arctic Ocean and Beaufort Gyre in Two Simulations With Different Horizontal Resolutions, Journal of Geophysical Research, 2019.

Isern-Fontanet, J., Garcia-Ladona, E., and Font, J.: Identification of Marine Eddies from Altimetric Maps, JOURNAL OF ATMOSPHERIC AND OCEANIC TECHNOLOGY, 20, 2003.

Karcher, M., Smith, J. N., Kauker, F., Gerdes, R., and Smethie, W. M.: Recent changes in Arctic Ocean circulation revealed by iodine-129 observations and modeling, Journal of Geophysical Research: Oceans, 117, https://doi.org/10.1029/2011JC007513, publisher: Blackwell Publishing Ltd, 2012.

Kozlov, I. E., Artamonova, A. V., Manucharyan, G. E., and Kubryakov, A. A.: Eddies in the Western Arctic Ocean From Space-borne SAR Observations Over Open Ocean and Marginal Ice Zones, Journal of Geophysical Research: Oceans, 124, 6601–6616, https://doi.org/10.1029/2019JC015113, 2019.

Kubryakov, A. A., Kozlov, I. E., and Manucharyan, G. E.: Large Mesoscale Eddies in the Western Arctic Ocean From Satellite Altimetry Measurements, Journal of Geophysical Research: Oceans, 126, e2020JC016 670, https://doi.org/10.1029/2020JC016670, 2021.

Lellouche, J.-M., Greiner, E., Le Galloudec, O., Garric, G., Regnier, C., Drevillon, M., Benkiran, M., Testut, C.-E., Bourdalle-Badie, R., Gasparin, F., Hernandez, O., Levier, B., Drillet, Y., Remy, E., and Le Traon, P.-Y.: Recent updates to the Copernicus Marine Service global ocean monitoring and forecasting real-time 112° high-resolution system, Ocean Science, 14, 1093–1126, https://doi.org/10.5194/os-14-1093-2018, 2018.

Levitus, S., Locarnini, R. A., Boyer, T. P., Mishonov, A. V., Antonov, J. I., Garcia, H. E., Baranova, O. K., Zweng, M. M., Johnson, D. R., and Seidov, D.: World ocean atlas 2009, Volume 1: Temperature, Tech. rep., U.S. Government Printing Office, Washington, D.C, 2010.

Li, J., Pickart, R. S., Lin, P., Bahr, F., Arrigo, K. R., Juranek, L., and Yang, X.: The Atlantic Water Boundary Current in the Chukchi Borderland and Southern Canada Basin, Journal of Geophysical Research: Oceans, 125, e2020JC016 197, https://doi.org/10.1029/2020JC016197, 2020.

Li, X., Wang, Q., Danilov, S., Koldunov, N., Liu, C., Müller, V., Sidorenko, D., and Jung, T.: Eddy activity in the Arctic Ocean projected to surge in a warming world, Nature Climate Change, https://doi.org/10.1038/s41558-023-01908-w, 2024.

Lique, C. and Johnson, H. L.: Is there any imprint of the wind variability on the Atlantic Water circulation within the Arctic Basin?, Geophysical Research Letters, 2015.

https://doi.org/10.5194/egusphere-2025-3527
Preprint. Discussion started: 30 July 2025

Lique, C., Johnson, H. L., and Davis, P. E. D.: On the Interplay between the Circulation in the Surface and the Intermediate Layers of the Arctic Ocean, JOURNAL OF PHYSICAL OCEANOGRAPHY, 45, 2015.

Liu, C., Wang, Q., Danilov, S., Koldunov, N., Müller, V., Li, X., Sidorenko, D., and Zhang, S.: Spatial Scales of Kinetic Energy in the Arctic Ocean, Journal of Geophysical Research: Oceans, 129, e2023JC020 013, https://doi.org/10.1029/2023JC020013, 2024.

MacKinnon, J. A., Simmons, H. L., Hargrove, J., Thomson, J., Peacock, T., Alford, M. H., Barton, B. I., Boury, S., Brenner, S. D., Couto, N., Danielson, S. L., Fine, E. C., Graber, H. C., Guthrie, J., Hopkins, J. E., Jayne, S. R., Jeon, C., Klenz, T., Lee, C. M., Lenn, Y.-D., Lucas, A. J., Lund, B., Mahaffey, C., Norman, L., Rainville, L., Smith, M. M., Thomas, L. N., Torres-Valdés, S., and Wood, K. R.: A warm jet in a cold ocean, Nature Communications, 12, 2418, https://doi.org/10.1038/s41467-021-22505-5, 2021.

Madec, G., Bell, M., Blaker, A., Bricaud, C., Bruciaferri, D., Castrillo, M., Calvert, D., Jérômeme Chanut, Clementi, E., Coward, A., Epicoco, I., Éthé, C., Ganderton, J., Harle, J., Hutchinson, K., Iovino, D., Lea, D., Lovato, T., Martin, M., Martin, N., Mele, F., Martins, D., Masson, S., Mathiot, P., Mocavero, S., Müller, S., Nurser, A. G., Paronuzzi, S., Peltier, M., Person, R., Rousset, C., Rynders, S., Samson, G., Téchené, S., Vancoppenolle, M., and Wilson, C.: NEMO Ocean Engine Reference Manual, https://doi.org/10.5281/ZENODO.1464816, publisher: Zenodo Version Number: v4.2.1, 2023.

Manley, T. O. and Hunkins, K.: Mesoscale eddies of the Arctic Ocean, Journal of Geophysical Research: Oceans, 90, 4911–4930, https://doi.org/10.1029/JC090iC03p04911, 1985.

Manucharyan, G. E. and Isachsen, P. E.: Critical Role of Continental Slopes in Halocline and Eddy Dynamics of the Ekman-Driven Beaufort Gyre, Journal of Geophysical Research: Oceans, 124, 2679–2696, https://doi.org/10.1029/2018JC014624, publisher: Blackwell Publishing Ltd, 2019.

Manucharyan, G. E. and Spall, M. A.: Wind-driven freshwater buildup and release in the Beaufort Gyre constrained by mesoscale eddies, Geophysical Research Letters, 43, 273–282, https://doi.org/10.1002/2015GL065957, 2016.

Manucharyan, G. E. and Thompson, A. F.: Heavy footprints of upper-ocean eddies on weakened Arctic sea ice in marginal ice zones, 2022.

Manucharyan, G. E. and Timmermans, M.-L.: Generation and Separation of Mesoscale Eddies from Surface Ocean Fronts, Journal of Physical Oceanography, 43, 2545–2562, https://doi.org/10.1175/JPO-D-13-094.1, 2013.

Manucharyan, G. E., Spall, M. A., and Thompson, A. F.: A Theory of the Wind-Driven Beaufort Gyre Variability, Journal of Physical Oceanography, 46, 3263–3278, https://doi.org/10.1175/JPO-D-16-0091.1, 2016.

Manucharyan, G. E., Lopez-Acosta, R., and Wilhelmus, M. M.: Spinning ice floes reveal intensification of mesoscale eddies in the western Arctic Ocean, Scientific Reports, 12, 7070, https://doi.org/10.1038/s41598-022-10712-z, 2022.

Martínez-Moreno, J., Lique, C., and Talandier, C.: Sea ice heterogeneity as a result of ocean eddy activity during the ice growth season, https://doi.org/10.22541/essoar.171405575.59826457/v2, 2024.

McLaughlin, F. A., Carmack, E. C., Williams, W. J., Zimmermann, S., Shimada, K., and Itoh, M.: Joint effects of boundary currents and thermohaline intrusions on the warming of Atlantic water in the Canada Basin, 1993–2007, Journal of Geophysical Research: Oceans, 114, 2008JC005 001, https://doi.org/10.1029/2008JC005001, 2009.

Meier, W. and Stroeve, J.: An Updated Assessment of the Changing Arctic Sea Ice Cover, Oceanography, https://doi.org/10.5670/oceanog.2022.114, 2022.

Meneghello, G., Marshall, J., Campin, J. M., Doddridge, E., and Timmermans, M. L.: The Ice-Ocean Governor: Ice-Ocean Stress Feedback Limits Beaufort Gyre Spin-Up, Geophysical Research Letters, 45, 11,293–11,299, https://doi.org/10.1029/2018GL080171, publisher: Blackwell Publishing Ltd, 2018.

https://doi.org/10.5194/egusphere-2025-3527
Preprint. Discussion started: 30 July 2025

Meneghello, G., Doddridge, E., Marshall, J., Scott, J., and Campin, J.-M.: Exploring the Role of the "Ice–Ocean Governor" and Mesoscale Eddies in the Equilibration of the Beaufort Gyre: Lessons from Observations, JOURNAL OF PHYSICAL OCEANOGRAPHY, 50, 2020.

Meneghello, G., Marshall, J., Lique, C., Isachsen, L. E., Doddridge, E., Campin, J.-M., Regan, H., and Talandier, C.: Genesis and Decay of Mesoscale Baroclinic Eddies in the Seasonally Ice-Covered Interior Arctic Ocean, JOURNAL OF PHYSICAL OCEANOGRAPHY, 51, 2021.

Meredith, M., Heywood, K., Dennis, P., Goldson, L., White, R., Fahrbach, E., Schauer, U., and Østerhus, S.: Freshwater fluxes through the Western Fram Strait, Geophysical Research Letters, 28, 1615–1618, https://doi.org/10.1029/2000GL011992, 2001.

Muilwijk, M., Hattermann, T., Martin, T., and Granskog, M. A.: Future sea ice weakening amplifies wind-driven trends in surface stress and Arctic Ocean spin-up, Nature Communications, 15, 6889, https://doi.org/10.1038/s41467-024-50874-0, 2024.

Nurser, A. J. G. and Bacon, S.: Arctic Ocean Rossby radius Eddy length scales and the Rossby radius in the Arctic Ocean Arctic Ocean Rossby radius, Ocean Sci. Discuss, 10, 1807–1831, https://doi.org/10.5194/osd-10-1807-2013, 2013.

Okubo, A.: Horizontal dispersion of floatable particles in the vicinity of velocity singularities such as convergences, Deep Sea Research and Oceanographic Abstracts, 17, 445–454, https://doi.org/10.1016/0011-7471(70)90059-8, 1970.

Pasquero, C., Provenzale, A., and Babiano, A.: Parameterization of dispersion in two-dimensional turbulence, Journal of Fluid Mechanics, 439, 279–303, https://doi.org/10.1017/S0022112001004499, 2001.

Pedlosky, J.: Geophysical Fluid Dynamics, springer edn., 1982.

Pickart, R. S., Weingartner, T. J., Pratt, L. J., Zimmermann, S., and Torres, D. J.: Flow of winter-transformed Pacific water into the Western Arctic, Deep Sea Research Part II: Topical Studies in Oceanography, 52, 3175–3198, https://doi.org/10.1016/j.dsr2.2005.10.009, 2005.

Planat, N., Tremblay, B., Dufour, C., and Straub, D.: Seasonal and decadal geostrophic pathways of Pacific and Atlantic Waters in the Arctic Amerasian Basin from observations, https://doi.org/10.22541/essoar.172124890.02099361/v1, 2024.

Regan, H. C., Lique, C., and Armitage, T. W. K.: The Beaufort Gyre Extent, Shape, and Location Between 2003 and 2014 From Satellite Observations, Journal of Geophysical Research, 2019.

Regan, H. C., Lique, C., Talandier, C., and Meneghello, G.: Response of Total and Eddy Kinetic Energy to the Recent Spinup of the Beaufort Gyre, JOURNAL OF PHYSICAL OCEANOGRAPHY, 50, 2020.

Rieck, J. K., Dufour, C. O., Nadeau, L.-P., and Thompson, A. F.: mesoscale eddies in an idealized Southern Ocean, 2024.

Rieck, J. K., Martínez-Moreno, J., Lique, C., Dufour, C., and Talandier, C.: Mean Kinetic Energy and its Projected Changes Dominate over Eddy Kinetic Energy in the Arctic Ocean, https://doi.org/10.22541/essoar.175244620.06508655/v1, 2025.

Spall, M. A., Pickart, R. S., Fratantoni, P. S., and Plueddemann, A. J.: Western Arctic Shelfbreak Eddies: Formation and Transport, Journal of Physical Oceanography, 38, 1644–1668, https://doi.org/10.1175/2007JPO3829.1, 2008.

Stadnyk, T. A., Tefs, A., Broesky, M., Déry, S. J., Myers, P. G., Ridenour, N. A., Koenig, K., Vonderbank, L., and Gustafsson, D.: Changing freshwater contributions to the Arctic, Elementa: Science of the Anthropocene, 9, 00 098, https://doi.org/10.1525/elementa.2020.00098, 2021.

Stegner, A., Le Vu, B., Dumas, F., Ghannami, M. A., Nicolle, A., Durand, C., and Faugere, Y.: Cyclone-Anticyclone Asymmetry of Eddy Detection on Gridded Altimetry Product in the Mediterranean Sea, Journal of Geophysical Research: Oceans, 126, e2021JC017 475, https://doi.org/10.1029/2021JC017475, 2021.

Talandier, C. and Lique, C.: CREG12.L75-REF12, https://doi.org/10.5281/ZENODO.13491948, 2024.

Toole, J., Krishfield, R., Timmermans, M.-L., and Proshutinsky, A.: The Ice-Tethered Profiler: Argo of the Arctic, Oceanography, 24, 126–135, https://doi.org/10.5670/oceanog.2011.64, 2011.

https://doi.org/10.5194/egusphere-2025-3527
Preprint. Discussion started: 30 July 2025

Tulloch, R., Marshall, J., Hill, C., and Smith, K. S.: Scales, Growth Rates, and Spectral Fluxes of Baroclinic Instability in the Ocean, Journal of Physical Oceanography, 41, 1057–1076, https://doi.org/10.1175/2011JPO4404.1, 2011.

Vancoppenolle, M., Rousset, C., Blockley, E., Aksenov, Y., Feltham, D., Fichefet, T., Garric, G., Guémas, V., Iovino, D., Keeley, S., Madec, G., Massonnet, F., Ridley, J., Schroeder, D., and Tietsche, S.: SI3, the NEMO Sea Ice Engine, https://doi.org/10.5281/ZENODO.7534900, publisher: Zenodo Version Number: 4.2release_doc1.0, 2023.

von Appen, W.-J., Baumann, T. M., Janout, M. A., Koldunov, N. V., Lenn, Y.-D., Pickart, R. S., and Wang, Q.: Eddies and the Distribution of Eddy Kinetic Energy in the Arctic Ocean, 35, 42–51, 2022.

Wang, Q., Koldunov, N. V., Danilov, S., Sidorenko, D., Wekerle, C., Scholz, P., Bashmachnikov, I. L., and Jung, T.: Eddy Kinetic Energy in the Arctic Ocean From a Global Simulation With a 1-km Arctic, Geophysical Research Letters, 47, https://doi.org/10.1029/2020GL088550, publisher: Blackwell Publishing Ltd, 2020.

Watanabe, E.: Beaufort shelf break eddies and shelf-basin exchange of Pacific summer water in the western Arctic Ocean detected by satellite and modeling analyses, Journal of Geophysical Research, 116, C08 034, https://doi.org/10.1029/2010JC006259, 2011.

Watanabe, E., Onodera, J., Harada, N., Honda, M. C., Kimoto, K., Kikuchi, T., Nishino, S., Matsuno, K., Yamaguchi, A., Ishida, A., and Kishi, M. J.: Enhanced role of eddies in the Arctic marine biological pump, Nature Communications, 5, 3950, https://doi.org/10.1038/ncomms4950, 2014.

Weiss, J.: The dynamics of enstrophy transfer in two-dimensional hydrodynamics, Physica D: Nonlinear Phenomena, 48, 273–294, https://doi.org/10.1016/0167-2789(91)90088-Q, 1991.

Woodgate, R. A.: Increases in the Pacific inflow to the Arctic from 1990 to 2015, and insights into seasonal trends and driving mechanisms from year-round Bering Strait mooring data, Progress in Oceanography, 160, 124–154, https://doi.org/10.1016/j.pocean.2017.12.007, publisher: Elsevier Ltd, 2018.

Zhang, J. and Rothrock, D. A.: Modeling Global Sea Ice with a Thickness and Enthalpy Distribution Model in Generalized Curvilinear Coordinates, Monthly Weather Review, 131, 845–861, https://doi.org/10.1175/1520-0493(2003)131<0845:MGSIWA>2.0.CO;2, 2003.

Zhao, M., Timmermans, M.-L., Cole, S., Krishfield, R., Proshutinsky, A., and Toole, J.: Characterizing the eddy field in the Arctic Ocean halocline, Journal of Geophysical Research: Oceans, 119, 8800–8817, https://doi.org/10.1002/2014JC010488, 2014.

Zhao, M., Timmermans, M. L., Cole, S., Krishfield, R., and Toole, J.: Evolution of the eddy field in the Arctic Ocean's Canada Basin, 2005–2015, Geophysical Research Letters, 43, 8106–8114, https://doi.org/10.1002/2016GL069671, publisher: Blackwell Publishing Ltd, 2016.